Table V. Dipole Moments of the Two Cumulene-Based Series (Debye)

molecule	X = O	X = S
$H_2C{=}X$	2.332[16]	1.647[16]
$H_2C{=}C{=}X$	1.422[16]	1.021[17]
$H_2C{=}C{=}C{=}X$	2.297[a,2]	2.064
$H_2C{=}C{=}C{=}C{=}X$	1.9767[18]	

[a] $\mu_a = 2.156$; $\mu_b = 0.791$.

progressions occur at frequencies lower than those of the ground state. Relative intensity measurements on the most intense $K_p = 2$ propadienethione vibrational satellite lines gives a frequency of $\sim$250 cm^{-1} for the lowest bending mode, which because of spin statistics arguments must be an out-of-plane motion. This frequency is close to that predicted by the ab initio calculations in Table III for both the in-plane and out-of-plane bends.

The dipole moment of 2.064 D for propadienethione is about the value expected when the trends in the dipole moments of the two cumulene series are examined as in Table V. The alternation in size of the dipole moment with odd and even numbers of carbon atoms is evident in both series.

Acknowledgment. Financial support by ARGS is acknowledged. We thank IBM Australia for access to their 3090 computer system under a joint research program.

Registry No. $H_2C_3{}^{34}S$, 112196-93-7; $H_2{}^{13}CC_2S$, 112196-92-6; $H_2C^{13}CCS$, 112196-91-5; DHC_3S, 112196-90-4; D_2C_3S, 112196-89-1; H_2C_3S, 83797-23-3; cyclopenteno-1,2,3-thiadiazole, 56382-73-1; (cyclopenteno-4,4-d_2)-1,2,3-thiadiazole, 112196-87-9; (cyclopenteno-4-d_1)-1,2,3-thiadiazole, 112196-88-0.

Phase Transition in the Conductive Molecular Crystals Bis(tetramethyltetraselenafulvalene)[bis(trifluoromethyl)-ethylene]diselenolatonickel and -platinum, $[TMTSF]_2[M(tds)_2]$, M = Ni, Pt. Relation to the Copper Analogue

William B. Heuer, Philip J. Squattrito, Brian M. Hoffman,* and James A. Ibers*

Contribution from the Department of Chemistry and Materials Research Center, Northwestern University, Evanston, Illinois 60208. *Received March 30, 1987*

Abstract: A series of quasi-two-dimensional molecular conductors with formula $[TMTSF]_2[M(tds)_2]$ (TMTSF = tetramethyltetraselenafulvalene; tds = [bis(trifluoromethyl)ethylene]diselenolato; M = Ni, Pt, Cu) are described. All have σ_{RT} = 20–100 Ω^{-1} cm^{-1} with metal-like character near room temperature. When M = Ni or Pt, there is a novel first-order structural transition (at T_c = 275 and 245 K, respectively) in which the low-temperature state exhibits enhanced conductivity; no corresponding transition occurs when M = Cu. At room temperature the three compounds are isostructural. The structure of M = Ni at 293 K consists of segregated stacks (along c) of TMTSF cations that are flanked by parallel chains of $M(tds)_2$ anions so as to form a two-dimensional anion–cation network parallel to the (010) plane. Crystal data: triclinic, space group C_i^1-$P\bar{1}$; a = 11.503 (18), b = 12.465 (20), c = 7.885 (13) Å; α = 96.39 (4), β = 109.57 (4), γ = 77.92 (4)°; V = 1040.7 Å^3; Z = 1. ESR and magnetic susceptibility measurements are consistent with the formulation $[(TMTSF)^{0.5+}]_2[[M(tds)_2]^-]$, where the anions have an open-shell, paramagnetic ($S = {}^1/_2$) configuration when M = Ni or Pt but are closed-shell and diamagnetic when M = Cu. Thus, the existence of a transition correlates with the electronic structure of the anion. The conductivity arises from a three-fourths-filled band associated with the TMTSF stacks; for M = Ni or Pt, the carrier spins are exchange-coupled to the localized anion moments. Interestingly, the structure of the low-temperature phase of M = Ni, determined at 116 K, is disordered; it is derived from the room-temperature structure by uncorrelated translations of the individual stacks and chains by $\pm{}^1/_8c$ along c. Crystal data: triclinic, space group C_i^1-$P\bar{1}$; a = 11.346 (21), b = 12.171 (34), c = 7.719 (11) Å; α = 95.30 (34), β = 108.75 (13), γ = 79.90 (25)°; V = 993.0 Å^3; Z = 1. The altered disposition of the stacks and chains in the disordered low-temperature structure enhances the intermolecular contacts within the two-dimensional anion–cation network.

In recent years, the field of molecular solid-state chemistry has experienced considerable growth fueled by the discovery of molecular crystals that exhibit metallic conductivity.[1,2] Of particular interest here are the organic superconductors,[3] which are salts of the heterofulvalene donor species tetramethyltetraselenafulvalene (TMTSF)[4] and bis(ethylenedithio)tetrathiafulvalene. The crystal structures of these compounds exhibit an enhanced multidimensional character, arising from intermolecular chalcogen–chalcogen interactions, that is believed to contribute substantially to the unusual physical properties.

The observation[5] that the nature of the anions plays an important role in modulating the dimensionality of such materials

(1) (a) Hatfield, W. E., Ed. *Molecular Metals*; Plenum: New York, 1979. (b) Devreese, J. T., Evrard, R. P., Van Doren, V. E., Eds. *Highly Conducting One-Dimensional Solids*; Plenum: New York, 1979. (c) Alcacer, L. *The Physics and Chemistry of Low Dimensional Solids*; NATO Advanced Study Institute Series C; Reidel: Dordrecht, 1980; Vol. 56. (d) Miller, J. S., Ed. *Extended Linear Chain Compounds*; Plenum: New York: 1982, Vol. 1 and 2; 1983, Vol. 3.

(2) (a) Miller, J. S., Epstein, A. J., Eds. *Ann. N.Y. Acad. Sci. U.S.A.* **1978**, *313*. (b) Epstein, A. J., Conwell, E. M., Eds. Proceedings of the International Conference on Low-Dimensional Conductors, Boulder, CO, 1981; *Mol. Cryst. Liq. Cryst.* **1982**, *79*; *Mol. Cryst. Liq. Cryst.* **1982**, *81*. (c) Comēs, R., Bernier, P., Andre, J. J., Rouxel, J., Eds. Proceedings of the International Conference on Low-Dimensional Conductors and Superconductors, Les Arcs, 1982; *J. Phys., Colloq.* **1983**, *C3*. (d) Pecile, C., Zerbi, G., Bozio, R., Girlando, A., Eds. Proceedings of the International Conference on the Physics and Chemistry of Low-Dimensional Synthetic Metals, Abano Terme, 1984; *Mol. Cryst. Liq. Cryst.* **1985**, *119*; *Mol. Cryst. Liq. Cryst.* **1985**, *120*.

(3) (a) Williams, J. M.; Beno, M. A.; Wang, H. H.; Leung, C. W.; Emge, T. J.; Geiser, U.; Carlson, K. D. *Acc. Chem. Res.* **1985**, *18*, 261–267. (b) Williams, J. M. *Prog. Inorg. Chem.* **1985**, *33*, 183–220.

(4) Abbreviations used in text: TMTSF, tetramethyltetraselenafulvalene; TTF, tetrathiafulvalene; TMPD, *N,N,N',N'*-tetramethyl-*p*-phenylenediamine; TCNQ, tetracyanoquinodimethane; $(TCNQ)Br_2$, 2,5-dibromotetracyanoquinodimethane; DMTM, *N,N*-dimethylthiomorpholinium; dmit, isotrithionedithiolate; mnt, maleonitriledithiolate; bds, *o*-benzenedithiolato; tds, bis(trifluoromethyl)ethylenediselenolato.

(5) Williams, J. M.; Beno, M. A.; Sullivan, J. C.; Banovetz, L. M.; Broam, J. M.; Blackman, G. S.; Carlson, C. D.; Greer, D. L.; Loesing, D. M. *J. Am. Chem. Soc.* **1983**, *105*, 643–644.

0002-7863/88/1510-0792$01.50/0

has intensified interest in the preparation of heterofulvalene donor-based compounds incorporating a wider variety of both organic and inorganic acceptors. In particular, a number of salts of planar metal bis(dithiolene) complex anions have been studied.[6,7] One of these, [TTF][Ni(dmit)$_2$]$_2$ (TTF = tetrathiafulvalene; dmit = isotrithionedithiolato),[7] was recently reported[7c] to exhibit a superconducting transition at 1.62 K (7-kbar hydrostatic pressure), making it the first molecular superconductor based on a transition-metal complex. Like the organic superconductors, [TTF][Ni(dmit)$_2$]$_2$ possesses a strongly multidimensional structure.

As an extension of our research on conductive molecular crystals based on metallomacrocyclic complexes,[8] we have prepared a series of heterofulvalene salts with metal bis(diselenolene) complex anions of the type [M(tds)$_2$]$^-$ (M = Ni, Pt, Cu; tds = [bis(trifluoromethyl)ethylene]diselenolato). We anticipated that these materials might exhibit stronger multidimensional interactions than in the comparable metal bis(dithiolene) compounds by virtue of the larger van der Waals radius and greater polarizability of selenium compared with sulfur.

This paper describes the preparation and physical characterization of an isostructural series of molecular conductors with formula [TMTSF]$_2$[M(tds)$_2$] (M = Ni, Pt, Cu). Previously, we reported[9] that the compounds with M = Ni or Pt show a novel transition to a low-temperature phase with enhanced conductivity. The macroscopic physical properties of these materials now are found to depend strongly on the metal ion; specifically, the phase transition observed when M = Ni or Pt does not occur when M = Cu. The details of the structural modification involved in this first-order phase transition have been elucidated by crystal structure determinations on the M = Ni derivative at temperatures above and below T_c. The observed metal dependence of the transition can be understood qualitatively through a consideration of the electronic structures of the constituent metal complex anions.

Experimental Section

Starting Materials. TMTSF (recrystallized grade) was obtained from Strem Chemical Co. and used as received. The monoanionic metal bis(diselenolene) complexes [M(tds)$_2$]$^-$ (M = Ni, Pt, Cu) were prepared as described elsewhere.[10] The complexes were used as their tetrabutylammonium (M = Ni) and tetraphenylphosphonium (M = Pt and Cu) salts. 1,1,2-Trichloroethane (Aldrich) was distilled from CaH_2 under nitrogen and stored over activated 4-Å molecular sieves.

Electrocrystallization Procedure. Crystals of [TMTSF]$_2$[M(tds)$_2$] (M = Ni, Pt, Cu) were obtained by the galvanostatic electrolysis of 1,1,2-trichloroethane solutions containing TMTSF (4×10^{-3} M) along with the appropriate monoanionic metal complex (2×10^{-3} M). A two-compartment cell similar to that described by Lee et al.[11] was employed. The platinum wire electrodes were soaked in HNO_3, rinsed thoroughly, and dried before use. A nitrogen atmosphere was maintained over the electrolysis solutions, and the cells were isolated from light, thermal fluctuations, and mechanical vibrations. A constant current ($i = 2 \times 10^{-6}$ A, current density 4×10^{-6} A cm^{-2}) was applied for a period of 10 days, after which the crystalline material formed on the anode was collected by filtration, washed with $CHCl_3$, and air dried. Elemental analysis results (Galbraith Laboratory, Knoxville, TN) for bulk samples of all three compounds were consistent with the formula [TMTSF]$_2$[M(tds)$_2$]. Anal. Calcd for $C_{28}H_{24}F_{12}Se_{12}Ni$: C, 21.08; H, 1.51; Se, 59.43; F, 14.30. Found: C, 20.86; H, 1.47; Se, 58.50; F, 14.18. Anal. Calcd for $C_{28}H_{24}F_{12}Se_{12}Pt$: C, 19.42; H, 1.39; Se, 54.75; F, 13.17. Found: C, 19.46; H, 1.42; Se, 54.34; F, 13.01. Anal. Calcd for $C_{28}H_{24}F_{12}Se_{12}Cu$: C, 21.01; H, 1.50; Se, 59.25; F, 14.26. Found: C, 20.96; H, 1.50; Se, 59.00; F, 14.04.

Single-Crystal Electrical Conductivity Studies. Crystals were mounted inside TO-5 integrated-circuit cans for ac conductivity measurements. The crystals were mounted across four parallel 8-μm graphite fibers (Alfa/Ventron) that were attached to the wire leads within the can. All electrical contacts were made with a conductive paste prepared by suspending palladium powder (0.25–0.55 μm, Alfa/Ventron) in an organic binder (Aero-Gloss 65-1 dope, Pactra Hobby, Van Nuys, CA). Sample resistance along the long crystal dimension was measured by a low-frequency (27-Hz) technique, as previously described.[12] The absolute conductivity of the sample was calculated according to $\sigma_\parallel = (1/\rho)L/A$, where ρ = sample resistivity, L = sample length between the measuring points, and A = cross-sectional area of the sample. Crystals mounted for conductivity studies were thin, elongated plates with average dimensions 1.0 mm × 0.05 mm × 0.03 mm. The uncertainty inherent in the determination of the geometric factor L/A for these crystals was estimated to be ca. ±20%. Relative conductivities for a specific sample are accurate to the level of the resistance measurement (±1%). The anisotropy of the conductivity ($\sigma_\parallel/\sigma_\perp$) for two relatively large single crystals (dimensions ca. 0.7 mm × 0.3 mm × 0.1 mm) was determined by procedures described by Montgomery.[13] In this case the electrical contacts were made directly to the Al leads of the TO-5 can with the use of silver paint (Du Pont No. 4929). Low temperatures were obtained with cold N_2 gas from liquid N_2 boiloff, and the temperature was monitored with a calibrated copper–constantan thermocouple anchored to the sample holder assembly within 1 cm of the sample.

Magnetic Susceptibility Measurements. Static magnetic susceptibilities were measured at a field of 10 kG over the temperature range 2–300 K with a SHE VTS-50 SQUID susceptometer. Sample holders were made of high-purity Spectrosil quartz (Thermal American, Inc.). Background measurements on empty sample holders were made over the full temperature range just prior to measurements on the samples. Sample mass for all runs was 40–60 mg. Raw data were corrected for holder background and sample core diamagnetism, which was calculated from Pascal's constants.[14]

ESR Measurements. X-band ESR measurements between 100–350 K were made with a highly modified Varian E-4 spectrometer with 100-kHz field modulation. The microwave frequency was measured with a Hewlett-Packard Model X532B frequency meter, and the magnetic field was calibrated with DPPH (2,2-diphenyl-1-picrylhydrazyl; g = 2.0036) as an external standard. Sample temperatures in this range were obtained with the use of cold N_2 gas and a Varian V6040 variable-temperature controller. Sample temperature was monitored with a calibrated copper–constantan thermocouple placed in the sample tube within 5 mm of the sample. Stability was better than ±1 K.

Low-temperature (5–100 K) ESR spectra at X-band frequencies were recorded with a Varian E-4 console interfaced with a Varian Model E102 microwave bridge and a Varian 9-in. magnet. The sample temperature was regulated by an Air Products Model LTR cryostat used in conjunction with a Scientific Instruments, Inc., Model 3700-APD-E digital temperature controller and was monitored by a calibrated silicon diode cryogenic temperature sensor (Lakeshore Cryotronics DT-500 DRC).

Q-band ESR measurements were performed at room temperature and ca. 130 K with a Varian E-109 spectrometer equipped with a Varian Model EC-1351 35-GHz conversion package. Low-temperature spectra were obtained by enclosing the cavity within a Varian Model EC-268 variable-temperature Dewar and cooling it with cold N_2 gas. Sample temperature was determined by placing a calibrated copper–constantan thermocouple beside the cavity in the cold gas flow.

Differential Scanning Calorimetry. DSC measurements over the range 175–400 K were performed on polycrystalline samples with a Perkin-Elmer DSC-2 calorimeter. The scan rate was 20° min^{-1}. Sample temperature calibration was referenced to the melting points of n-heptane (182.54 K), mercury (234.28 K), and gallium (302.43 K). Approximate transition enthalpies (ΔH_t) were determined by crude integration of the DSC peaks from precisely weighed samples, with the melting transition of indium metal (ΔH_t = 6.80 cal g^{-1}) used as a reference standard.

(6) (a) Kato, R.; Mori, T.; Kobayashi, A.; Sasaki, Y.; Kobayashi, H. *Chem. Lett.* **1984**, 1–4. (b) Kato, R.; Kobayashi, H.; Kobayashi, A.; Sasaki, Y. *Ibid.* **1985**, 131–134. (c) Kobayashi, H.; Kato, R.; Kobayashi, A.; Sasaki, Y. *Ibid.* 191–194. (d) *Ibid.* 535–538. (e) Underhill, A. E.; Tonge, J. S.; Clemenson, P. I. *Mol. Cryst. Liq. Cryst.* **1985**, *125*, 439–446. (f) Kobayashi, H.; Kato, R.; Mori, T.; Kobayashi, A.; Sasaki, Y.; Saito, G.; Inokuchi, H. *Ibid.* 125–134. (g) Kobayashi, A.; Sasaki, Y.; Kato, R.; Kobayashi, H. *Chem. Lett.* **1986**, 387–390.

(7) (a) Bousseau, M.; Valade, L.; Bruniquel, M.-F.; Cassoux, P.; Garbauskas, M.; Interrante, L.; Kasper, J. *Nouv. J. Chim.* **1984**, *8*, 3–6. (b) Valade, L.; Legros, J.-P.; Bousseau, M.; Cassoux, P.; Garbauskas, M.; Interrante, L. V. *J. Chem. Soc., Dalton Trans.* **1985**, 783–794. (c) Brossard, L.; Ribault, M.; Bousseau, M.; Valade, L.; Cassoux, P. *C. R. Acad. Sci., Ser. 2* **1986**, *302*, 205–210.

(8) Hoffman, B. M.; Ibers, J. A. *Acc. Chem. Res.* **1983**, *16*, 15–21.

(9) Heuer, W. B.; Hoffman, B. M. *J. Chem. Soc., Chem. Commun.* **1986**, 174–175.

(10) Heuer, W. B.; True, A. E.; Swepston, P. N.; Hoffman, B. M., submitted for publication in *Inorg. Chem.*

(11) Lee, M. M.; Stokes, J. P.; Wiygul, F. W.; Kistenmacher, T. J.; Cowan, D. O.; Poehler, T. O.; Bloch, A. N.; Fuller, W. W.; Gubsen, D. U. *Mol. Cryst. Liq. Cryst.* **1982**, *79*, 145–154.

(12) Phillips, T. E.; Anderson, J. R.; Schramm, C. J.; Hoffman, B. M. *Rev. Sci. Instrum.* **1979**, *50*, 263–275.

(13) Montgomery, H. C. *J. Appl. Phys.* **1971**, *42*, 2971–2975.

(14) Mulay, L. N. *Magnetic Susceptibility*; Wiley-Interscience: New York, 1963; pp 1779–1782.

Table I. Summary of Crystal Data and Intensity Collection Parameters

formula	$NiSe_{12}C_{28}F_{12}H_{24}$	
mol wt	1594.71	
space group	C_i^1-$P\bar{1}$	
a, Å	11.503 (18)	11.346 (21)
b, Å	12.465 (20)	12.171 (34)
c, Å	7.885 (13)	7.719 (11)
α, deg	96.39 (4)	95.30 (34)
β, deg	109.57 (4)	108.75 (13)
γ, deg	77.92 (4)	79.90 (25)
V, Å^3	1040.7	993.0
Z	1	
T of data collcn, K	293	116[a]
cryst vol, mm^3	0.0028	
cryst shape	slab elongated along [001] and bound by {100}, {010}, {001}, (11$\bar{1}$)	
radiatn	graphite-monochromatized Mo Kα (λ(Kα_1) = 0.7093 Å)	
linear abs coeff, cm^{-1}	109.3	119.2
transmissn factors[b]	0.225–0.547	0.214–0.517
detector aperture, mm		
horizontal	6.6	4.6
vertical	6.0	6.0
	32 cm from crystal	
takeoff angle, deg	3.0	
scan type[c]	ω: 1°/min	ω-step scan: 1-s count per 0.03° step
scan range, deg	−1.5 to +0.90 in ω	−1.95 to +1.05 in ω
λ^{-1} sin θ limits, Å^{-1}	0.0369–0.4822	0.0369–0.5958
	1.5 ≤ θ(Mo Kα_1) ≤ 20°	1.5 ≤ θ(Mo Kα_1) ≤ 25°
bkgd counts	20 s at each end of scan	
data collcd	$\pm h,\pm k,\pm l$	
p factor	0.04	
no. of unique data	1953	2602
no. of unique data with $F_o^2 > 3\sigma(F_o^2)$	1241	1062
no. of variables	241	278
$R(F^2)$	0.063	0.143
$R_w(F^2)$	0.089	0.138
R (on F for $F_o^2 > 3\sigma(F_o^2)$)	0.036	0.052
error in obsn of unit wt, e^2	1.16	1.19

[a] The low-temperature system for the Picker FACS-1 diffractometer is based on a design by: Huffman, J. C. Ph.D. Thesis, Indiana University, 1974. [b] The analytical method as employed in the Northwestern Absorption Program, AGNOST, was used for the absorption correction: de Meulenaer, J.; Tompa, H. *Acta Crystallogr.* **1965**, *19*, 1014. [c] The Picker FACS-1 diffractometer was operated under the Vanderbilt disk-oriented system: Lenhert, P. G. *J. Appl. Crystallogr.* **1975**, *8*, 568.

Crystallographic Studies. Examination of Weissenberg X-ray photographs indicated that crystals of $[TMTSF]_2[Ni(tds)_2]$ belong to the triclinic system. On the basis of the satisfactory residual of 0.019 obtained from averaging the Friedel pairs of the absorption-corrected room-temperature data for which $F_o^2 > 3\sigma(F_o^2)$ (vide infra), we favor the centrosymmetric space group C_i^1-$P\bar{1}$. The cell parameters were determined at room temperature from least-squares analysis[15] of 14 reflections in the range 10° ≤ 2θ(Mo Kα_1) ≤ 29° that had been automatically centered on a Picker FACS-1 X-ray diffractometer. The refined cell constants and additional relevant crystal data are given in Table I.

Owing to the mosaicity of the crystals, intensity data were collected at room temperature with the ω-scan technique. The intensities of six standard reflections, measured at 100 reflection intervals throughout the data collection, exhibited no significant fluctuations. All calculations were performed on a Harris 1000 computer with programs and methods standard for this laboratory.[16] Atomic scattering factors and anomalous dispersion terms were taken from the usual sources.[17] The unique Ni atom and the six independent Se atoms were located from a Patterson map. All C and F atoms were located from subsequent electron density syntheses. The 12 independent H atoms were located from a difference electron density map. The H atom positions were idealized (C–H = 0.95 Å) and included in subsequent calculations as fixed contributions to F_c. The thermal parameter of a given H atom was fixed at 1.0 Å^2 greater than the equivalent isotropic thermal parameter of the C atom to which it is attached. The unit cell contains one $Ni(tds)_2$ anion and two independent TMTSF cations. As the Ni atom of the anion and the central C–C bond on each of the TMTSF cations rest on inversion centers, the asymmetric unit contains half of the $Ni(tds)_2$ anion and half of two TMTSF cations. The final cycle of refinement was performed on all 1953 unique F_o^2 values and included anisotropic thermal parameters for all non-hydrogen atoms. The final values for R and R_w on F_o^2 are 0.063 and 0.089, respectively, while the conventional R index for the 1241 data with $F_o^2 > 3\sigma(F_o^2)$ is 0.036. An analysis of F_o^2 vs F_c^2 as a function of F_o^2, λ^{-1} sin θ, and Miller indices reveals no unusual trends. The final difference electron density map shows no features with height greater than 3% that of an Se atom. The anisotropic thermal parameters of the F atoms are consistent with substantial oscillation of the perfluoromethyl groups about the C–CF_3 axes.

Table II. Positional Parameters and Equivalent Isotropic Thermal Parameters for $[TMTSF]_2[Ni(tds)_2]$ (Room-Temperature Structure)

atom	x	y	z	B_{eq}, Å^2
Ni(1)	0	0	0	3.54 (8)
Se(1)	−0.05467 (13)	0.10521 (12)	−0.23973 (19)	4.22 (5)
Se(2)	−0.06798 (13)	0.14070 (12)	0.16915 (20)	4.30 (5)
Se(3)	0.29900 (12)	0.07929 (12)	0.50217 (20)	4.29 (5)
Se(4)	0.44119 (12)	−0.15980 (12)	0.34914 (19)	4.13 (5)
Se(5)	0.30516 (12)	0.08771 (11)	0.01288 (19)	4.02 (5)
Se(6)	0.42791 (12)	−0.15479 (11)	−0.15085 (19)	4.11 (5)
F(1)	0.1102 (14)	−0.37959 (94)	−0.2627 (16)	14.7 (7)
F(2)	0.1582 (17)	−0.44896 (88)	−0.0366 (18)	16 (1)
F(3)	0.2790 (11)	−0.3830 (12)	−0.0860 (27)	19 (1)
F(4)	0.27729 (79)	−0.38616 (73)	0.3117 (12)	7.3 (4)
F(5)	0.1701 (12)	−0.29068 (89)	0.4530 (14)	12.0 (6)
F(6)	0.09159 (88)	−0.40212 (86)	0.2590 (15)	10.1 (5)
C(1)	0.1211 (10)	−0.2429 (10)	0.1568 (19)	3.3 (5)
C(2)	0.1236 (10)	−0.2584 (11)	−0.0147 (19)	3.7 (5)
C(3)	0.1655 (18)	−0.3628 (13)	−0.0993 (24)	5.9 (7)
C(4)	0.1628 (15)	−0.3299 (14)	0.2882 (21)	5.0 (7)
C(5)	0.4703 (11)	0.04847 (97)	−0.4674 (17)	4.0 (5)
C(6)	0.3029 (13)	0.2229 (11)	−0.3928 (17)	4.2 (5)
C(7)	0.4128 (12)	0.2580 (11)	−0.3335 (17)	4.0 (5)
C(8)	0.4314 (14)	0.3676 (12)	−0.2438 (20)	5.8 (6)
C(9)	0.1789 (13)	0.2872 (11)	−0.3852 (19)	5.2 (6)
C(10)	0.4747 (11)	0.04956 (94)	0.0332 (16)	3.5 (5)
C(11)	0.3203 (12)	0.2300 (10)	0.1195 (16)	3.6 (5)
C(12)	0.4334 (12)	0.2572 (11)	0.1788 (16)	3.6 (5)
C(13)	0.4633 (12)	0.3637 (11)	0.2712 (18)	4.4 (5)
C(14)	0.2000 (11)	0.2987 (11)	0.1326 (17)	4.3 (5)
H1C(8)	0.518	0.371	−0.196	6.8
H2C(8)	0.390	0.425	−0.325	6.8
H3C(8)	0.398	0.380	−0.144	6.8
H1C(14)	0.215	0.354	0.227	5.1
H2C(14)	0.152	0.334	0.022	5.1
H3C(14)	0.150	0.254	0.158	5.1
H1C(13)	0.537	0.351	0.380	5.1
H2C(13)	0.484	0.407	0.196	5.1
H3C(13)	0.396	0.406	0.308	5.1
H1C(9)	0.188	0.347	−0.298	6.0
H2C(9)	0.127	0.316	−0.501	6.0
H3C(9)	0.132	0.240	−0.354	6.0

Final atomic parameters for the room-temperature structure are provided in Table II. Final anisotropic thermal parameters and structure amplitudes are available as supplementary material.[18]

In preparation for the low-temperature X-ray study, the temperature of the crystal on the Picker FACS-1 diffractometer was decreased from 293 to ~116 K at a rate of 2 K min^{-1}. The most readily apparent evidence of a structural change upon cooling was a dramatic decrease in intensity of several strong reflections with l = 2. This observation was confirmed by taking Polaroid rotation photographs about the c axis of another crystal of the compound mounted on an Enraf-Nonius CAD4 diffractometer. The photographs, taken at room temperature and at 196 K, clearly reveal that at 196 K the l = 2 layer line is diminished in intensity relative to the l = 0 and 1 lines. There was no evidence of a

(15) Corfield, P. W. R.; Doedens, R. J.; Ibers, J. A. *Inorg. Chem.* **1967**, *6*, 197–204.
(16) For example: Waters, J. M.; Ibers, J. A. *Inorg. Chem.* **1977**, *16*, 3273–3277.
(17) Cromer, D. T.; Waber, J. T. *International Tables for X-ray Crystallography*; Kynoch: Birmingham, England, 1974; Vol. IV, Table 2.2A. Cromer, D. T. *Ibid.* Table 2.3.1.
(18) Supplementary material. See paragraph at end of paper.

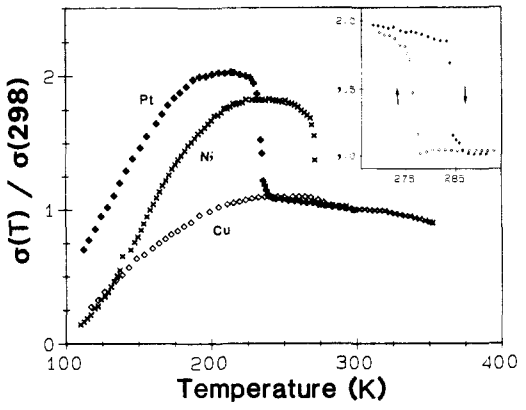

Figure 1. Four-probe, single-crystal conductivities of $[TMTSF]_2[M(tds)_2]$ (M = Ni, Pt, Cu) taken along the needle axis as a function of temperature. Conductivity values are normalized to σ_{RT} = 18.7, 61.2, and 63.2 Ω^{-1} cm^{-1} for M = Ni, Pt, and Cu, respectively. Inset: hysteresis upon temperature cycling through the phase transition in $[TMTSF]_2[Ni(tds)_2]$.

larger cell in these photographs. In addition, rotation photographs taken about the *a* and *b* axes of the crystal used in the X-ray studies showed no superstructure spots below the transition temperature, which has been shown from electrical conductivity measurements to be about 275 K (vide infra).

Unit cell parameters at 116 K were determined from least-squares analysis of 14 reflections in the range 22° ≤ 2θ(Mo Kα$_1$) ≤ 28° automatically centered on a Picker FACS-1 X-ray diffractometer. The refined cell constants and other relevant data for the low-temperature study are given in Table I.

Intensity data were collected at 116 K with the use of ω step scans, where the step interval was 0.03°, the counting time was 1 s/step, and the total scan width was 3°. The intensities of six standard reflections, measured at 100 reflection intervals, were stable throughout the course of data collection. The change in collection technique from the room-temperature study was necessitated by a general broadening of diffraction peaks, attributable to an increase in the mosaicity as the crystal was cooled. Examination of the diffraction behavior of the crystal after the data collection indicates, however, that it sustained no catastrophic damage upon going through the transition. Indeed, a comparison of unit cell parameters and the intensities of approximately 50 strong low-angle reflections collected at room temperature before and after the low-temperature X-ray study confirms that the phase transition is fully reversible, in keeping with the observed physical properties of this material. Nevertheless, the increase in mosaicity is not reversible; there is a general decrease in the quality of the crystal after the phase transition.

A less satisfactory residual of 0.068 is obtained from averaging the absorption corrected Friedel pairs ($F_o^2 > 3\sigma(F_o^2)$) of the low-temperature data set. We attribute the poorer agreement to the diminished crystal quality. We believe that the centrosymmetric nature of the room-temperature structure is maintained in the low-temperature structure. All calculations were performed as for the room-temperature study. The structure was solved by a combination of Patterson and direct methods (MULTAN). The Ni and Se atoms were located from an E map while the C and F atoms were located from ensuing electron density syntheses. The large number of these peaks and their positions in the unit cell indicate a disordered structure. In the low-temperature unit cell, the centers of the metal anion and both TMTSF cations have moved off the crystallographic centers of symmetry. As a result, the asymmetric unit contains at fixed occupancies of 50% an entire $Ni(tds)_2$ anion and two TMTSF cations. No attempt was made to locate the H atoms. A full anisotropic refinement of all non-hydrogen atoms was attempted; several half-carbon atoms displayed anisotropic thermal parameters that were *not* positive definite. The data are not of sufficient quality to allow such a model to be used. Accordingly, the final cycle of refinement was performed on F_o^2 with the 2602 unique data; it included anisotropic thermal parameters for the Ni and Se atoms and isotropic thermal parameters for the C and F atoms. The final *R* indices on F_o^2 are R = 0.143 and R_w = 0.138; the conventional *R* index on F_o for the 1062 data for which $F_o^2 > 3\sigma(F_o^2)$ is 0.052. No unusual trends are observed from an analysis of F_o^2 vs F_c^2 as a function of F_o^2, $\lambda^{-1}\sin\theta$, and Miller indices. The largest feature in the final difference electron density map is <6% of the height of an Se atom. The unexceptional anisotropic thermal parameters for the Ni and Se atoms support the model of disorder of the structure.

Final atomic parameters for all non-hydrogen atoms are given in Table III. Anisotropic thermal parameters and structure amplitudes are provided as supplementary material.[18]

Table III. Positional Parameters and Equivalent Isotropic Thermal Parameters for $[TMTSF]_2[Ni(tds)_2]$ (Low-Temperature Structure)

atom	*x*	*y*	*z*	B_{eq}, Å^2
Ni(1)	−0.00342 (39)	0.00032 (39)	0.36985 (57)	1.70 (9)
Se(1)	0.05795 (28)	−0.11285 (27)	0.16076 (41)	1.9 (1)
Se(2)	−0.05481 (28)	0.13721 (27)	0.17375 (39)	1.64 (9)
Se(3)	−0.06120 (29)	0.11180 (28)	0.59232 (46)	1.9 (1)
Se(4)	0.05390 (30)	−0.13982 (29)	0.57695 (46)	2.2 (1)
Se(5)	0.57833 (27)	0.15669 (27)	0.52793 (41)	1.09 (9)
Se(6)	0.30775 (27)	0.08448 (27)	0.38136 (42)	0.98 (8)
Se(7)	0.69919 (31)	−0.09067 (30)	0.35402 (44)	1.7 (1)
Se(8)	0.42432 (31)	−0.15624 (29)	0.21091 (45)	1.8 (1)
Se(9)	0.29940 (32)	0.07871 (32)	0.13266 (47)	2.0 (1)
Se(10)	0.56871 (31)	0.15601 (29)	0.28459 (45)	1.7 (1)
Se(11)	0.43467 (29)	−0.16588 (28)	−0.03020 (42)	1.25 (9)
Se(12)	0.69843 (28)	−0.08110 (27)	0.12318 (42)	1.18 (9)
F(1)	0.2722 (17)	−0.3953 (17)	0.6417 (27)	4.4 (5)
F(2)	0.1144 (14)	−0.4583 (14)	0.4232 (19)	2.2 (3)
F(3)	0.0834 (16)	−0.3721 (17)	0.6649 (24)	3.5 (4)
F(4)	0.0753 (14)	−0.4075 (14)	0.0759 (20)	2.5 (3)
F(5)	0.1941 (13)	−0.3034 (13)	0.0227 (18)	1.8 (3)
F(6)	0.2689 (15)	−0.4099 (15)	0.2558 (21)	3.0 (4)
F(7)	−0.2698 (15)	0.3890 (15)	0.1148 (20)	2.7 (3)
F(8)	−0.0878 (14)	0.3696 (14)	0.0818 (21)	2.5 (3)
F(9)	−0.1198 (15)	0.4581 (16)	0.3116 (21)	3.0 (4)
F(10)	−0.0848 (14)	0.4125 (14)	0.6767 (20)	2.0 (3)
F(11)	−0.2708 (14)	0.4080 (14)	0.4846 (22)	2.3 (3)
F(12)	−0.1981 (16)	0.3005 (16)	0.7188 (22)	2.9 (4)
C(1)	0.4758 (31)	0.0592 (30)	0.4109 (43)	2.7 (7)
C(2)	0.5252 (23)	−0.0447 (23)	0.3476 (33)	0.6 (5)
C(3)	0.3313 (30)	0.2310 (29)	0.5116 (41)	2.7 (7)
C(4)	0.4323 (35)	0.2528 (35)	0.5588 (50)	3.6 (8)
C(5)	0.5572 (22)	−0.2639 (21)	0.1841 (31)	0.1 (4)
C(6)	0.6859 (22)	−0.2350 (22)	0.2603 (32)	0.6 (5)
C(7)	0.2057 (30)	0.2967 (31)	0.5286 (42)	4.7 (8)
C(8)	0.4762 (23)	0.3597 (24)	0.6697 (32)	1.3 (5)
C(9)	0.5241 (24)	−0.3732 (23)	0.1080 (34)	1.5 (5)
C(10)	0.7935 (21)	−0.3056 (21)	0.2365 (30)	0.0 (4)
C(11)	0.4760 (23)	0.0431 (23)	0.1488 (33)	0.7 (5)
C(12)	0.5302 (26)	−0.0551 (24)	0.0769 (35)	1.4 (6)
C(13)	0.3107 (22)	0.2250 (22)	0.2295 (31)	0.2 (5)
C(14)	0.4368 (23)	0.2581 (23)	0.3022 (32)	0.7 (5)
C(15)	0.5909 (28)	−0.2624 (28)	−0.0489 (41)	2.2 (6)
C(16)	0.6880 (33)	−0.2241 (33)	0.0015 (47)	3.6 (8)
C(17)	0.1947 (21)	0.2888 (21)	0.2415 (30)	0.2 (4)
C(18)	0.4545 (24)	0.3707 (24)	0.3807 (34)	1.4 (5)
C(19)	0.5575 (21)	−0.3701 (20)	−0.1587 (30)	0.6 (4)
C(20)	0.8252 (31)	−0.2854 (30)	0.0018 (42)	3.0 (7)
C(21)	0.1136 (24)	−0.2653 (25)	0.4447 (36)	1.5 (6)
C(22)	0.1052 (25)	−0.2466 (25)	0.2558 (35)	1.5 (5)
C(23)	−0.1143 (23)	0.2568 (23)	0.2953 (32)	1.0 (5)
C(24)	−0.1202 (22)	0.2520 (22)	0.4709 (35)	1.0 (5)
C(25)	0.1445 (32)	−0.3745 (33)	0.5343 (48)	3.8 (8)
C(26)	0.1592 (31)	−0.3381 (31)	0.1526 (45)	3.2 (7)
C(27)	−0.1509 (30)	0.3724 (30)	0.1893 (42)	2.8 (7)
C(28)	−0.1719 (24)	0.3436 (24)	0.5854 (36)	1.4 (5)

Results

Conductivity Measurements. Variable-temperature (100–300 K) four-probe measurements of the electrical conductivity along the needle axis of $[TMTSF]_2[M(tds)_2]$ (M = Ni, Pt, Cu) single crystals have been performed. The absolute room-temperature conductivities ($\sigma_\parallel$) for all three compounds are the same within experimental error, falling within the range 20–100 Ω^{-1} cm^{-1} for all crystals measured. All three compounds exhibit metal-like behavior ($d\sigma/dT < 0$) near room temperature. However, there are dramatic differences in the temperature dependence of the electrical conductivities (Figure 1).

M = Cu. The conductivity of $[TMTSF]_2[Cu(tds)_2]$ exhibits a broad plateau centered at 250 K, followed by activated behavior below ca. 225 K. Arrhenius plots of the data below 200 K are nonlinear; they yield a small, temperature-dependent activation energy with a limiting value of ca. 0.05 eV at the lowest temperature studied (100 K). The observed temperature dependence of the conductivity can be fit to eq 1,[19] where α = 3.25–3.30 and

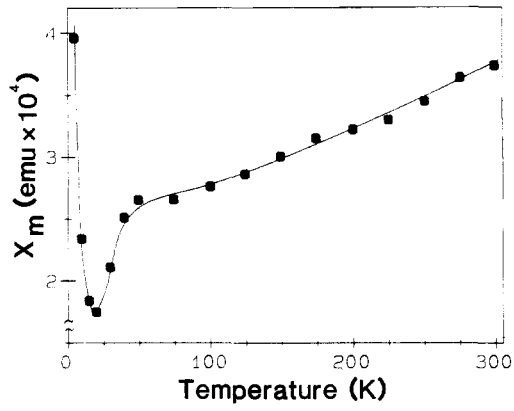

Figure 2. Molar static magnetic susceptibility of polycrystalline $[TMTSF]_2[Cu(tds)_2]$ as a function of temperature.

Δ = 800–850 K, depending upon the sample (A is a normalization constant).

$$\sigma(T) = AT^{-\alpha} \exp(-\Delta/T) \quad (1)$$

M = Ni, Pt. The temperature-dependent conductivities of single crystals of the Ni and Pt derivatives (Figure 1) exhibit an unusual feature: below the metal-like regime there is a transition in which the conductivity abruptly *increases*. The transition temperature, T_c, is different for M = Ni (270–275 K) and M = Pt (235–240 K); the range of T_c values indicated reflects the influence of variable crystal quality upon the transition. The conductivity of the low-temperature state immediately below the transition is generally 1.5–2.0 times greater than that of the corresponding high-temperature state, depending upon the sample. Further below the transition, the conductivities of the Ni and Pt derivatives reach broad maxima centered at 230 and 210 K, respectively, followed by activated behavior at lower temperatures. Arrhenius plots of the data are linear below 150 K; they yield limiting activation energies of 0.07 eV (M = Ni) and 0.03 eV (M = Pt) at 100 K.

When crystals of the Ni and Pt compounds are rewarmed, they undergo a reverse transition at a critical temperature T_c' that is higher than T_c (inset, Figure 1). The hysteresis ($T_c' - T_c > 0$) associated with the transition is sample dependent, falling in the range 10–20 K for all samples measured. Slow temperature cycling through the transition region retraces the cooling and warming curves, confirming the reversible nature of the transition.

The anisotropy of the electrical conductivity ($\sigma_\parallel/\sigma_\perp$) for two samples of $[TMTSF]_2[Ni(tds)_2]$ was evaluated by the Montgomery method;[13] crystals of the other derivatives suitable for such measurements could not be obtained. Here $\sigma_\parallel$ refers to the absolute conductivity along the crystallographic c axis, while $\sigma_\perp$ refers to the conductivity along [100]. The measured anisotropies for the two Ni crystals at 300 K were $\sigma_\parallel/\sigma_\perp$ = 23 and 34, a low value (average 28) indicative of a highly two-dimensional electronic structure. For example, this anisotropy is more than 1 order of magnitude smaller than the value $\sigma_\parallel/\sigma_\perp \sim 300$ found[20] for the quasi-two-dimensional metal $[TMTSF]_2[PF_6]$. When the crystals are cooled through the 275 K phase transition, both $\sigma_\parallel$ and $\sigma_\perp$ increase by a comparable amount, their ratio remaining unchanged (31 and 40 at 252 K) within experimental error.

Magnetic Susceptibility Measurements. The temperature dependence of the static magnetic susceptibilities of powder samples of $[TMTSF]_2[M(tds)_2]$ (M = Ni, Pt, Cu) has been studied over the range 2–300 K. In keeping with the conductivity results, the compounds exhibit two distinct types of behavior depending upon the identity of the central metal ion. The results indicate that the $[M(tds)_2]^-$ ions retain their monoanionic character upon incorporation into these compounds.

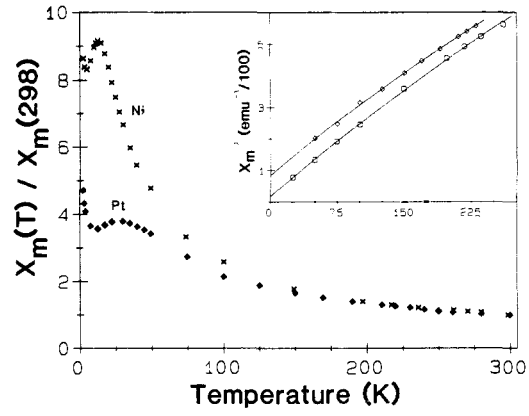

Figure 3. Molar static magnetic susceptibilities of $[TMTSF]_2[M(tds)_2]$ (M = Ni, Pt) as a function of temperature. Susceptibilities are normalized to $\chi_{RT} = 1.56 \times 10^{-3}$ and 1.47×10^{-3} emu mol^{-1} for M = Ni and Pt, respectively. Inset: plots of χ^{-1} vs T for M = Ni (□) and M = Pt (◇); solid lines represent best fits of the data to eq 2, as discussed in text.

M = Cu. The static magnetic susceptibility of $[TMTSF]_2[Cu(tds)_2]$, measured at 300 K and corrected for molecular core diamagnetism, is 3.74×10^{-4} emu mol^{-1}, which is comparable to the value of 4.2×10^{-4} emu mol^{-1} reported[20] for $[TMTSF]_2[PF_6]$. The measured susceptibility at 50 K is 70% of its room-temperature value (Figure 2). Such behavior is typical of the Pauli paramagnetism associated with mobile charge carriers in molecular conductors and is consistent with the formulation $[TMTSF^{0.5+}]_2[Cu(tds)_2^-]$, where the Cu complex is monoanionic and diamagnetic. An abrupt decrease in the susceptibility occurs below 50 K, suggesting that the charge carriers on the TMTSF stacks become localized and magnetically coupled at this temperature; preliminary conductivity measurements down to 10 K, however, fail to show a corresponding change in the transport properties. Below ca. 20 K, the weak residual susceptibility of the compound is obscured by a Curie tail ascribed to impurity or defect spins: a plot of χ^{-1} vs T for $T \leq 20$ K yields $C = 4.7 \times 10^{-3}$ emu K mol^{-1}, which corresponds to a 1% concentration of an $S = {}^1/_2$, $g = 2$ spin.

M = Ni, Pt. The $[M(tds)_2]^-$ (M = Ni, Pt) anions are paramagnetic ($S = {}^1/_2$) and, as expected, the magnetic behavior of the $[TMTSF]_2[M(tds)_2]$ (M = Ni, Pt) compounds differs from that of the Cu homologue. Their susceptibilities are much larger (M = Ni, $\chi = 1.56 \times 10^{-3}$ emu mol^{-1} at 298 K; M = Pt, $\chi = 1.47 \times 10^{-3}$ emu mol^{-1} at 300 K), and they increase strongly as the samples are cooled (Figure 3). Detailed examination of the temperature response of the susceptibility of the Pt compound (not shown) discloses a small anomaly in the same temperature range (ca. 245 K) where the conductivity transition is observed; a similar, though even less pronounced, feature appears near 280 K in the data for the Ni compound. The susceptibility of each compound in its low-temperature phase increases steadily as the temperature is decreased, reaching maxima at T_m = 13 K (M = Ni) and 28 K (M = Pt) and then diminishing rapidly. As for the Cu compound, the low-temperature behavior is largely obscured by a Curie tail arising from 1–2% of impurity or defect spins; subtraction of this impurity contribution shows a nonzero intercept at T = 0 K. The form of the susceptibility curve, with a broad maximum and nonzero intercept, is reminiscent of the behavior predicted[21] for an antiferromagnetic one-dimensional Heisenberg chain.

In the temperature range above T_c but below T_m, the susceptibilities of both the Ni and Pt compounds obey eq 2, where $\chi_c(T)$

$$\chi_o(T) = \chi_c(T) + \chi_\pi = C/(T - \Theta) + \chi_\pi \quad (2)$$

is the Curie–Weiss contribution from the spins localized on the complex anions and χ_π is the temperature-independent Pauli

(19) Epstein, A. J.; Conwell, E. M.; Sandman, D. J.; Miller, J. S. *Solid State Commun.* **1977**, *23*, 355–358.

(20) Bechgaard, K.; Jacobsen, C. S.; Mortensen, K.; Pedersen, H. J.; Thorup, N. *Solid State Commun.* **1980**, *33*, 1019–1125.

(21) (a) Bonner, J. C.; Fisher, M. E. *Phys. Rev.* **1964**, *135*, 640–658. (b) Hatfield, W. E.; Estes, W. E.; Marsh, W. E.; Pickens, M. W.; ter Haar, L. W.; Weller, R. R. In Reference 1d, Vol. 3, pp 43–142.

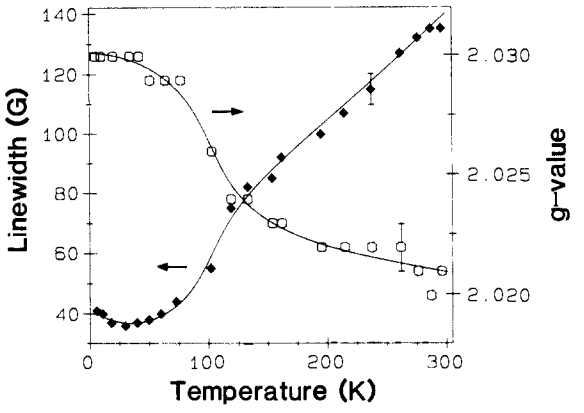

Figure 4. Temperature dependence of the ESR line width (◆) and g value of the zero crossing of the derivative signal (□) for polycrystalline $[TMTSF]_2[Cu(tds)_2]$. Error bars indicate the estimated uncertainty in the measurement of line widths and g values from the spectra.

susceptibility associated with the mobile carrier spins on the TMTSF stacks. Nonlinear least-squares fits of χ_o^{-1} vs T were performed with use of the data taken well above T_m (inset, Figure 3). The results are the following: M = Ni ($25 \leq T \leq 260$ K), $C = 0.406$ (8) emu K mol^{-1}, $\Theta = -7.3$ (8) K, $\chi_\pi = 2.3$ (3) $\times 10^{-4}$ emu mol^{-1}; M = Pt ($50 \leq T \leq 230$ K), $C = 0.40$ (2) emu K mol^{-1}, $\Theta = -34$ (5) K, $\chi_\pi = 2.9$ (8) $\times 10^{-4}$ emu mol^{-1}. The observed Curie constants, C, are close to the value expected for one spin per complex anion; for example, the value of 0.406 (8) (M = Ni) is in good agreement with that of 0.418 emu K mol^{-1} for one spin per $[Ni(tds)_2]^-$ ion calculated from eq 3, where N is Avogadro's

$$C = S(S + 1)(Ng^2\mu_B^2/3k) \quad (3)$$

number, μ_B is the Bohr magneton, k is Boltzmann's constant, $S = {}^1/_2$ is the electron spin, and $g^2 = 4.412$ is the average g^2 value for the $[Ni(tds)_2]^-$ ion.[22] The large negative values of Θ reflect the antiferromagnetic interactions among the anions in the low-temperature phase that cause the decrease in χ at $T < T_m$; the magnitudes of the temperature-independent components, χ_π, are reasonably close to the experimentally observed value of 3.74×10^{-4} emu mol^{-1} for M = Cu.

Electron Spin Resonance Measurements. ESR spectra of microcrystalline samples of $[TMTSF]_2[M(tds)_2]$ (M = Ni, Cu) were obtained at X-band frequency (ca. 9 GHz) over the temperature range 5–350 K and Q-band frequency (ca. 35 GHz) at room temperature and 130 K. The corresponding M = Pt derivative lacked a detectable ESR signal at either frequency and all temperatures investigated.

M = Cu. At X-band frequency the room-temperature powder ESR spectrum of $[TMTSF]_2[Cu(tds)_2]$ consists of a broad (peak-to-peak line width $\Delta H_{pp} = 130$ G) isotropic line centered at $g = 2.021$. This value is comparable to room-temperature g values of $\langle g \rangle = 2.020$ for $[TMTSF]_2[ClO_4]$ and $\langle g \rangle = 2.021$ for $[TMTSF]_2[PF_6]$, both of which have $\Delta H_{pp} > 200$ G at room temperature.[23] The g value for $TMTSF^+$ in solution is 2.029.[24]

As the temperature is lowered, the ESR line shape remains symmetric down to ca. 120 K; the g value of the zero crossing of the derivative signal (g_{cross}) remains essentially constant, while ΔH_{pp} decreases monotonically over the same temperature range (Figure 4). Below 120 K, the signal shows a partial resolution of the g anisotropy, which results in an abrupt increase in the measured g_{cross} and concomitant decrease in the apparent ΔH_{pp}, to ca. 2.03 and ca. 40 G, respectively, at 75 K. The values of g_{cross} and ΔH_{pp} undergo no further changes between 75 and 5 K, remaining fixed at $g_{cross} \cong g_\perp$ with ΔH_{pp} set by the g anisotropy; thus, further cooling produces only a reduction of the component widths and hence improved resolution of the g anisotropy at a constant pattern width.

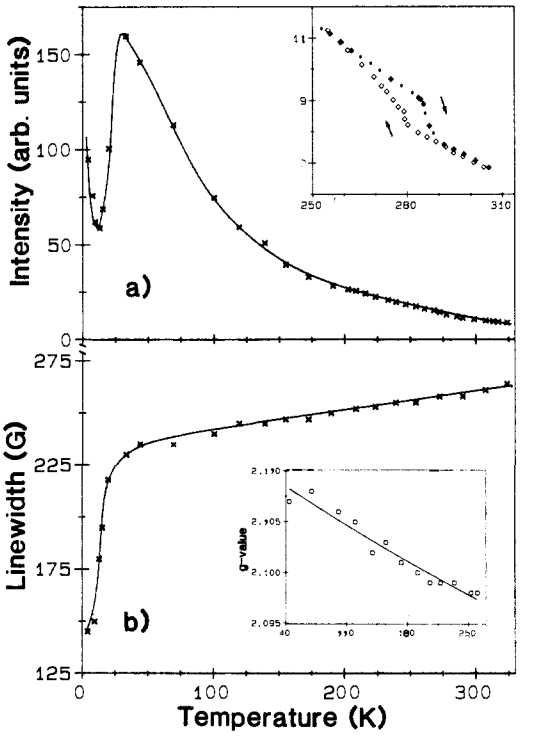

Figure 5. (a) Peak-to-peak ESR intensity (I_{pp}) for polycrystalline $[TMTSF]_2[Ni(tds)_2]$ as a function of temperature. Inset: temperature response of I_{pp} in the region of the first-order structural transition showing hysteresis that is observed upon temperature cycling. (b) ESR line width for polycrystalline $[TMTSF][Ni(tds)_2]$ as a function of temperature. Inset: temperature dependence of the g value for polycrystalline $[TMTSF]_2[Ni(tds)_2]$; solid line represents best fit of the data to eq 4, as discussed in text.

At Q-band frequency the signal is asymmetric at room temperature; at 130 K, it is fully resolved into an axially symmetric pattern with $g_\parallel = 1.991$ and $g_\perp = 2.032$. A similar g anisotropy has been observed in single-crystal ESR studies on the Bechgaard salts:[23] for $[TMTSF]_2[ClO_4]$, $g_{xx} = 1.990$, $g_{yy} = 2.039$, and $g_{zz} = 2.032$ (in the present powder spectra, the individual components of $g_\perp$ are apparently not resolved). These results confirm that the ESR signal and associated paramagnetism in $[TMTSF]_2[Cu(tds)_2]$ arise from charge carriers on the TMTSF stacks.

M = Ni. The room-temperature ESR spectrum of polycrystalline $[TMTSF]_2[Ni(tds)_2]$ at X-band frequency shows a single, symmetrical resonance at $g = 2.090$. The peak-to-peak line width is ca. 265 G, nearly twice that of the copper derivative. The temperature dependence of the ESR spectrum also is strikingly different: below room temperature the peak intensity (I_{pp}) of the signal increases, but the line width decreases only slightly (at 200 K, $\Delta H_{pp} = 250$ G) (Figure 5). The temperature dependence of I_{pp} shows an anomaly over the same temperature region where the conductivity transition is observed. Temperature cycling of the ESR sample in the vicinity of this anomaly (inset, Figure 5a) reproduces the hysteretic effect observed in the conductivity data, confirming its intrinsic character.

Both the ESR intensity and line width show effects (Figure 5) correlated with the maximum observed in the static susceptibility. As the temperature is lowered, the intensity increases smoothly down to $T \cong 30$ K and then decreases strongly with further cooling; in the same temperature range there is a sharp reduction in line width.

The g value of the resonance (g_{obsd}) gradually increases as the sample is cooled below room temperature (inset, Figure 5b). For the low-temperature phase g_{obsd} has been fit over the temperature range 50–250 K to a model of exchange coupling between two

(22) The X-band ESR spectrum of microcrystalline $[(C_4H_9)_4N][Ni(tds)_2]$ at 77 K yields the following values: $g_1 = 2.008$, $g_2 = 2.108$, $g_3 = 2.182$, and $g^2 = (g_1^2 + g_2^2 + g_3^2)/3 = 4.412$.

(23) Flandrois, S.; Coulon, C.; Delhaes, P.; Chasseau, D.; Hauw, C.; Gaultier, J.; Fabre, J. M.; Giral, L. *Mol. Cryst. Liq. Cryst.* **1982**, *79*, 307–319.

(24) Taranoka, Y.; Kanamori, J. *Conf. Ser.–Inst. Phys.* **1977**, *No. 39*, 588.

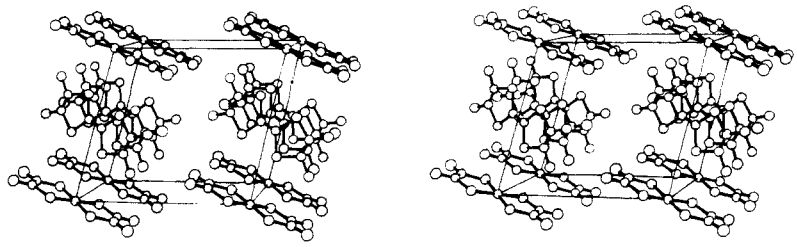

Figure 6. Stereoview of the molecular packing within the unit cell of the room-temperature $[TMTSF]_2[Ni(tds)_2]$ structure, viewed down the c axis. F and H atoms have been omitted for clarity.

discrete spin systems that have different temperature-dependent spin susceptibilities (eq 4). Here $f_c(T) = [C/(T - \Theta)]/[C/(T - \Theta) + \chi_\pi]$ and $f_p(T) = 1 - f_c(T)$ are the fractional susceptibilities of the Curie–Weiss and Pauli spin systems, respectively; g_c and g_p are adjustable parameters corresponding to the average g values of the isolated spin systems. Using values of C, Θ, and χ_π determined independently from the fit of the static susceptibility data to eq 2 over this same temperature range (vide supra), we find $g_c = 2.111$ (2) and $g_p = 2.01$ (2). The value of g_c is close to the value $\langle g \rangle = 2.108$ observed[10] for the $[Ni(tds)_2]^-$ ion in solution. This suggests that the Curie–Weiss spins in $[TMTSF]_2[Ni(tds)_2]$ are associated with the complex anions. Similarly, the calculated value g_p is comparable to the g value found for the TMTSF-based spins in $[TMTSF]_2[Cu(tds)_2]$.

$$g_{obsd} = f_c(T)g_c + f_p(T)g_p \quad (4)$$

The Q-band spectrum of polycrystalline $[TMTSF]_2[Ni(tds)_2]$ at 130 K exhibits a rhombic pattern ($g_1 = 2.011$, $g_2 = 2.109$, $g_3 = 2.201$) that is highly characteristic of the $[Ni(tds)_2]^-$ ion.[22] Since, according to eq 2 and 4, the Curie–Weiss spins account for 93% of the total paramagnetic susceptibility of this compound at 130 K (i.e., $f_c(130\ K) = 0.93$), this result provides confirmation that the Curie–Weiss spins are associated with the complex anions.

Differential Scanning Calorimetry Measurement. DSC thermograms have been recorded for $[TMTSF]_2[M(tds)_2]$ (M = Ni, Pt, Cu) over the temperature range 175–400 K. As expected, the Cu derivative shows no evidence of a structural transition in this region. The Ni and Pt homologues both give well-defined endotherms upon warming at a rate of 20 K min^{-1}, with T_c' = 282.7 and 252.5 K, respectively. These values are consistent with the corresponding warming T_c's determined from ESR and conductivity measurements. When these samples are cooled at the same rate, extremely broad, unresolved exotherms associated with the reverse transition are observed; this sluggishness of the cooling transition prevented the determination of the associated T_c values. Repeated temperature cycling of the samples reproduces this behavior, confirming the reversible nature of the phase transition.

Approximate transition enthalpies, ΔH_t, have been determined by integration of the DSC peaks: M = Ni, $\Delta H_t = 0.49$ cal g^{-1}; M = Pt, $\Delta H_t = 0.23$ cal g^{-1}. These results are comparable to the value $\Delta H_t = 0.66$ cal g^{-1} found[25] for the structural phase transition in the organic conductor $[(C_6H_5)_3P(CH_3)][TCNQ]_2$ (TCNQ = tetracyanoquinodimethane).

X-ray Crystallography. Weissenberg photographs of the three compounds (M = Ni, Pt, Cu) are superimposable at room temperature; hence, the compounds are isostructural. To elucidate the structural basis of the phase transition in these materials, complete structure determinations were performed on a $[TMTSF]_2[Ni(tds)_2]$ single crystal both above (298 K) and below (116 K) its transition temperature.

Room-Temperature Crystal Structure of $[TMTSF]_2[Ni(tds)_2]$. At room temperature crystals of $[TMTSF]_2[Ni(tds)_2]$ are triclinic, space group C_i^1-$P\bar{1}$. The molecular packing within the unit cell is shown in Figure 6.

The geometry of the TMTSF cations (Figure 7; Table IV) is similar to that commonly observed in conducting TMTSF compounds; they are arranged in segregated stacks containing multiple

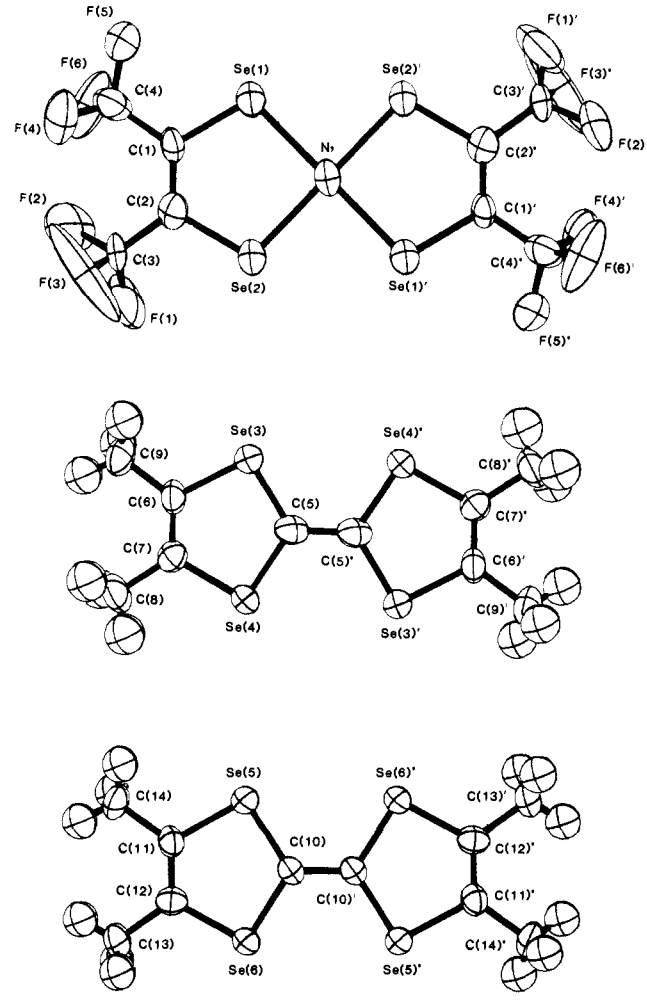

Figure 7. View onto the planes of the symmetry-independent molecules in the room-temperature $[TMTSF]_2[Ni(tds)_2]$ structure showing the atom-numbering scheme. Ellipsoids are drawn at the 50% probability level.

intrastack Se–Se contacts shorter than 4.0 Å, the van der Waals contact distance for selenium.[26,27] Stacking is along the crystallographic c axis, which corresponds to the longest crystal dimension and the direction of highest electrical conductivity. The stacks are composed of alternating, symmetry-independent centrosymmetric TMTSF cations, hereafter designated A and A′, that lie on the inversion centers ($^1/_2$, 0, 0) and ($^1/_2$, 0, $^1/_2$), respectively. The overlap of the nearly planar TMTSF cations within a stack is of the usual "double bond over ring" type, with

(25) Iida, Y. *Bull. Chem. Soc. Jpn.* **1970**, *43*, 3685–3688.

(26) Pauling, L. *The Nature of the Chemical Bond*, 3rd ed.; Cornell University: Ithaca, 1960; p 260.

(27) Previous work (cf. ref 33) indicates that the 4.0-Å limit is a reasonable standard by which to judge electronically significant Se–Se contacts in conducting TMTSF compounds; since the nature of the structure suggests that overlap considerations are favorable, we shall adopt this standard in the ensuing discussion and will hereafter designate Se–Se contacts ≤4.0 Å as "short".

Table IV. Selected Interatomic Distances (Å) and Angles (deg) for $[TMTSF]_2[Ni(tds)_2]$ (Room-Temperature Structure)

Ni(1)–Se(1)	2.258 (3)	Se(1)–Ni(1)–Se(2)	92.4 (1)
Ni(1)–Se(2)	2.252 (3)	C(1)–Se(1)–Ni(1)	103.4 (4)
Se(1)–Se(2)	3.121 (5)	C(2)–Se(2)–Ni(1)	103.1 (5)
Se(1)–Se(2)	3.256 (6)	Se(1)–C(1)–C(4)	115 (1)
Se(1)–C(1)	1.87 (1)	Se(1)–C(1)–C(2)	120 (1)
Se(2)–C(2)	1.88 (1)	C(2)–C(1)–C(4)	125 (1)
C(1)–C(2)	1.35 (2)	Se(2)–C(2)–C(1)	121 (1)
C(1)–C(4)	1.48 (2)	Se(2)–C(2)–C(3)	114 (1)
C(2)–C(3)	1.46 (2)	C(3)–C(2)–C(1)	126 (1)
C(3)–F(1)	1.25 (2)	Se(4)–Se(3)–Se(4)	89.7 (1)
C(3)–F(2)	1.26 (2)	C(5)–Se(3)–C(6)	93.7 (6)
C(3)–F(3)	1.25 (2)	C(5)–Se(4)–C(7)	93.4 (6)
C(4)–F(4)	1.32 (2)	Se(3)–C(5)–Se(4)	115.3 (6)
C(4)–F(5)	1.32 (2)	C(5)–C(5)–Se(3)	123 (1)
C(4)–F(6)	1.29 (2)	C(5)–C(5)–Se(4)	121 (1)
Se(3)–Se(4)	3.156 (5)	Se(3)–C(6)–C(7)	119 (1)
Se(3)–Se(4)	3.391 (4)	Se(3)–C(6)–C(9)	115 (1)
Se(3)–C(5)	1.86 (1)	C(7)–C(6)–C(9)	126 (1)
Se(3)–C(6)	1.89 (1)	Se(4)–C(7)–C(6)	119 (1)
Se(4)–C(5)	1.87 (1)	Se(4)–C(7)–C(8)	116 (1)
Se(4)–C(7)	1.89 (1)	C(6)–C(7)–C(8)	125 (1)
C(5)–C(5)	1.39 (2)	Se(6)–Se(5)–Se(6)	90.0 (1)
C(6)–C(7)	1.34 (2)	C(10)–Se(5)–C(11)	93.4 (5)
C(6)–C(9)	1.50 (2)	C(10)–Se(6)–C(12)	93.3 (5)
C(7)–C(8)	1.49 (2)	Se(5)–C(10)–Se(6)	115.4 (6)
Se(5)–Se(6)	3.154 (5)	C(10)–C(10)–Se(5)	123 (1)
Se(5)–Se(6)	3.371 (5)	C(10)–C(10)–Se(6)	122 (1)
Se(5)–C(10)	1.86 (1)	Se(5)–C(11)–C(12)	118 (1)
Se(5)–C(11)	1.89 (1)	Se(5)–C(11)–C(14)	114 (1)
Se(6)–C(10)	1.87 (1)	C(12)–C(11)–C(14)	127 (1)
Se(6)–C(12)	1.88 (1)	Se(6)–C(12)–C(11)	119 (1)
C(10)–C(10)	1.38 (2)	Se(6)–C(12)–C(13)	115 (1)
C(11)–C(12)	1.33 (1)	C(11)–C(12)–C(13)	126 (1)
C(11)–C(14)	1.50 (2)		
C(12)–C(13)	1.49 (2)		

a slight (2–3°) torsional distortion. Although the molecular planes of adjacent TMTSF cations within a stack are not constrained by symmetry to be parallel, the least-squares planes (defined by the four selenium atoms) of adjacent TMTSF molecules within a stack nonetheless are found to be so, within <1°. The resulting stacking architecture is similar to that found in such compounds as [TMTSF][TCNQ][28] and $[TMTSF]_2[(TCNQ)Br_2]$ ($(TCNQ)Br_2$ = 2,5-dibromotetracyanoquinodimethane).[29]

The centrosymmetric $[Ni(tds)_2]^-$ anions (Figure 7; Table IV) are essentially planar, with an average Ni–Se bond length of 2.255 (3) Å; this compares favorably with the 2.259-Å Ni–Se distance reported[30] for $[(C_4H_9)_4N]_2[Ni(bds)_2]$ (bds = *o*-benzenediselenolato), the only other structurally characterized nickel-bis(diselenolene) compound. The metrical parameters of the tds ligand are similar to those found in the other structurally characterized complexes of this ligand, $[Mo(tds)_2]$[31] and $[(C_6H_5)_4P][Pt(tds)_2]$.[10] The thermal ellipsoids of the fluorine atoms are significantly elongated, indicating a substantial degree of rotational freedom of the CF_3 groups at 293 K.

The TMTSF stacks within the crystal can be viewed as forming extended, sheetlike arrays that are parallel to (100) and sandwiched between layers of $[Ni(tds)_2]^-$ anions; the least-squares planes of the anions and cations are perpendicular within experimental error. The layers of $[Ni(tds)_2]^-$ anions parallel to the *b*–*c* plane can be viewed as being assembled from chains along *c*, within which the metal complexes abut edge-to-edge. A similar arrangement of anions and cations is found for the related metal–bis(dithiolene) compound $[TMPD]_2[Ni(mnt)_2]$ (TMPD = *N,N,N′,N′*-tetramethyl-*p*-phenylenediamine; mnt = maleonitriledithiolato);[32] as in that compound there are no short intermolecular contacts between adjacent anions within a chain (minimum interanion d_{Se-Se} = 4.680 (2) Å).

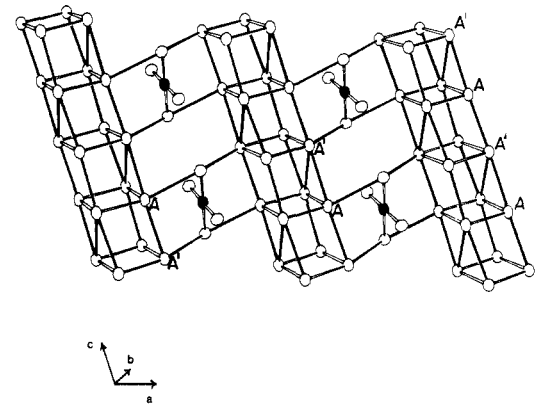

Figure 8. View onto the *a*–*c* plane of the room-temperature $[TMTSF]_2[Ni(tds)_2]$ structure, with all atoms except Ni (●) and Se (○) omitted. Intermolecular contacts ≤4.0 Å are drawn as solid lines to emphasize the two-dimensional character of the structure.

Viewed from the above perspective, the structure bears a resemblance to that found for the family of TMTSF-based superconductors[3] (the so-called Bechgaard salts) but with important differences. In particular, unlike the Bechgaard salts, the stacks of TMTSF molecules within a sheet abut corner-to-corner with contacts between CH_3 groups of adjacent stacks, rather than side-by-side with close interstack Se–Se contacts. The arrangement reported here precludes strong electronic interactions between adjacent TMTSF stacks within a sheet, as found in the Bechgaard phase.[33] There are, however, two distinct types of short anion–cation Se–Se contacts, with d_{Se-Se} = 3.917 (6) and 3.901 (5) Å. These contacts link each TMTSF cation to one $[Ni(tds)_2]^-$ anion in each of the neighboring chains displaced to either side along *a*; conversely, each anion contacts two cations within each of the two flanking stacks. A more realistic view of the structure therefore appears to be one in which the TMTSF stacks are tied together by the intervening complex anions within the *a*–*c* plane to form a two-dimensional molecular network (Figure 8). This unprecedented type of anion–cation network contrasts sharply with the interactions in the Bechgaard salts, in which the layers of anions act as insulating spacers between the homogeneous two-dimensional TMTSF sheets.

It is instructive to consider at this point the extended nature of the anion–cation Se–Se contacts within the *a*–*c* plane. For example, each $[Ni(tds)_2]^-$ anion is linked through contacts with neighboring TMTSF molecules to four other anions (related to the first by the translations $x + 1, y, z$; $x - 1, y, z$; $x + 1, y, z + 1$; and $x - 1, y, z - 1$, respectively) belonging to the nearest neighboring chains within the *a*–*c* plane. Two of these anion–cation–anion contacts extend laterally (i.e., both anions are at the same level along *c*), and two are diagonal (i.e., the anions are at different levels along *c*). Each TMTSF cation is likewise linked through the intervening anions to four cations within neighboring stacks, but the cation–anion–cation contacts are inequivalent for the two symmetry-independent types of TMTSF cations. Thus, whereas each A-type cation has both lateral and diagonal cation–anion–cation contacts, the A′ type has only diagonal ones. Because every ion within the room-temperature structure participates in such diagonal interactions, the extended $(anion–cation)_x$ network within the *a*–*c* plane is inherently two-dimensional.

Low-Temperature Crystal Structure of $[TMTSF]_2[Ni(tds)_2]$. As illustrated schematically in Figure 9, the structure of the low-

(28) Bechgaard, K.; Kistenmacher, T. J.; Bloch, A. N.; Cowan, D. O. *Acta Crystallogr., Sect. B: Struct. Crystallogr. Cryst. Chem.* **1977**, *B33*, 417–422.
(29) Stokes, J. P.; Emge, T. J.; Bryden, W. A.; Chappell, J. S.; Cowan, D. O.; Poehler, T. O.; Bloch, A. N.; Kistenmacher, T. J. *Mol. Cryst. Liq. Cryst.* **1982**, *79*, 327–336.
(30) Sandman, D. J.; Stark, J. C.; Acampora, L. A.; Samuelson, L. A.; Allen, G. W.; Jansen, S.; Jones, M. T.; Foxman, B. M. *Mol. Cryst. Liq. Cryst.* **1984**, *107*, 1–17.
(31) Pierpont, C. G.; Eisenberg, R. *J. Chem. Soc. A* **1971**, 2285–2289.
(32) Hove, M. J.; Hoffman, B. M.; Ibers, J. A. *J. Chem. Phys.* **1972**, *56*, 3490–3502.
(33) Whangbo, M.-H.; Williams, J. M.; Beno, M. A.; Dorfman, J. R. *J. Am. Chem. Soc.* **1983**, *105*, 646–648.

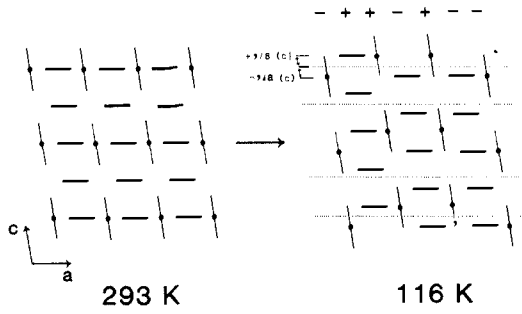

Figure 9. Schematic representation of the structural modification that occurs within the a–c plane of the $[TMTSF]_2[Ni(tds)_2]$ structure upon cooling through the 275 K phase transition. The TMTSF cations are symbolized by solid rectangles, while the anions are represented by circles with solid lines through them. The +/− notation used to indicate the direction of stack or chain displacements corresponds to that used in the text.

Table V. Selected Interatomic Distances (Å) and Angles (deg) for $[TMTSF]_2[Ni(tds)_2]$ (Low-Temperature Structure)

Ni(1)–Se(1)	2.228 (9)	Se(1)–Ni(1)–Se(2)	87.9 (3)
Ni(1)–Se(2)	2.228 (9)	Se(2)–Ni(1)–Se(3)	94.0 (3)
Ni(1)–Se(3)	2.280 (9)	Se(3)–Ni(1)–Se(4)	85.6 (3)
Ni(1)–Se(4)	2.310 (10)	Se(4)–Ni(1)–Se(1)	92.4 (3)
Se(1)–Se(2)	3.094 (10)	Se(4)–Ni(1)–Se(2)	178.7 (3)
Se(2)–Se(3)	3.299 (7)	Se(1)–Ni(1)–Se(3)	177.8 (3)
Se(3)–Se(4)	3.119 (10)	Se(5)–Se(6)–Se(8)	90.8 (3)
Se(4)–Se(1)	3.275 (7)	Se(5)–Se(7)–Se(8)	88.9 (3)
Se(5)–Se(6)	3.163 (8)	Se(6)–Se(5)–Se(7)	89.4 (3)
Se(5)–Se(7)	3.426 (11)	Se(6)–Se(8)–Se(7)	90.9 (3)
Se(7)–Se(8)	3.175 (9)	Se(9)–Se(10)–Se(12)	90.6 (3)
Se(6)–Se(8)	3.333 (11)	Se(9)–Se(11)–Se(12)	89.0 (3)
Se(9)–Se(10)	3.178 (9)	Se(10)–Se(9)–Se(11)	89.1 (3)
Se(9)–Se(11)	3.427 (11)	Se(10)–Se(12)–Se(11)	91.2 (3)
Se(10)–Se(12)	3.327 (11)		
Se(11)–Se(12)	3.163 (9)		

temperature phase is derived from the room-temperature structure by randomly translating the individual TMTSF stacks and $[Ni(tds)_2]^-$ chains along the crystallographic c axis by a distance of $\pm^1/_8c$ from their room-temperature positions. As we could find no evidence for a larger cell, we assume that the translations of the intact stacks and chains relative to one another are uncorrelated. The resulting structure belongs to the same space group C_i^1-$P\bar{1}$) as the room-temperature structure, but the individual molecules within the unit cell no longer reside on centers of symmetry.

A detailed analysis of individual molecular geometries for the low-temperature structure is precluded by the quality of the refinement, but it is nonetheless clear that the basic structural features of the TMTSF and $[Ni(tds)_2]^-$ ions (Figure 10; Table V) are essentially unaffected by the phase transition. For example, the four Se atoms within each anion and cation remain nearly coplanar, though they are no longer required by symmetry to be so. As expected, the observed isotropic thermal parameters of the fluorine atoms (Table III) are significantly reduced from the corresponding room-temperature values (Table II), indicating that the motional freedom of the CF_3 groups is largely curtailed at 116 K.

The basic architecture of the individual TMTSF stacks in the low-temperature structure is very similar to that seen at room temperature. Within the anion sheets, however, the chains of $[Ni(tds)_2]^-$ ions along c are significantly altered from their room-temperature form. The least-squares planes of the anions and cations remain essentially perpendicular, but each anion is rotated by ca. 11° about the plane normal passing through its central nickel atom. This rotation brings the long axis of each $[Ni(tds)_2]^-$ ion more nearly parallel to the planes of the neighboring TMTSF molecules within the a–c plane. Although the reorientation of the anions is accompanied by a contraction of the minimum interanion Se–Se distance within a chain to 4.448 (8) Å, this is still well beyond the van der Waals contact distance.

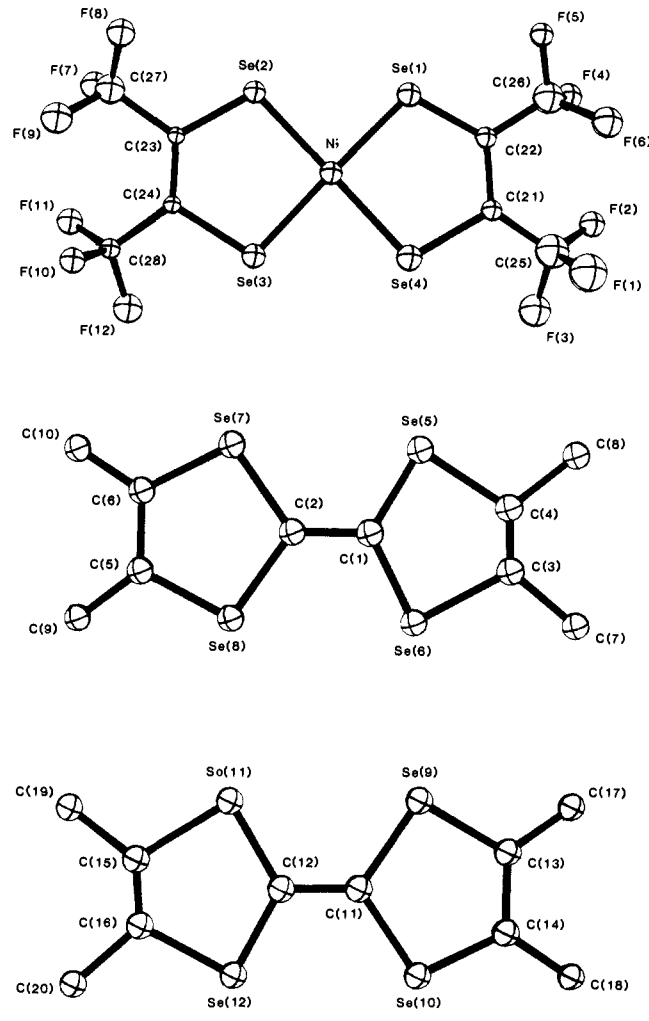

Figure 10. View onto the planes of the symmetry-independent molecules in the low-temperature $[TMTSF]_2[Ni(tds)_2]$ structure showing the atom-numbering scheme. Atoms in the anion are drawn as spheres corresponding to the equivalent isotropic thermal parameters listed in Table III; those of the cations are drawn as spheres of arbitrary size.

The uncorrelated translation of the TMTSF stacks and $[Ni(tds)_2]^-$ chains, together with the reorientation of the anions, creates new types of anion–cation Se–Se contacts that alter the character of the two-dimensional structural network in the low-temperature phase. The disordered nature of the low-temperature structure furthermore implies the presence of several crystallographically distinct local environments for the stacks and chains below the phase transition. These features are readily illustrated by an analysis of the structural disorder within the a–c plane.

The individual TMTSF stacks and anion chains retain their internal order along c in the low-temperature phase, and therefore each can be treated as a monolithic structural element. Each such element of the low-temperature structure can adopt either of two positions along c, corresponding to a translation of $+^1/_8c$ or $-^1/_8c$ from its room-temperature position; we symbolically denote these two allowed positions as + and −, respectively. All possible combinations of nearest-neighbor interactions within the a–c plane can then be generated by arbitrarily choosing one element as a fixed reference within the structure and systematically permutating the neighboring elements through their allowed positions along c relative to this reference. In the following discussion, we take the reference to be + and distinguish it with brackets, i.e. [+].

The interactions of a [+] reference stack (or chain) with the two neighboring chains (or stacks) within the a–c plane give rise to four distinct local environments that may be symbolized using an obvious notation: (+[+]+), (+[+]−), (−[+]+), and (−[+]−). Two of these, (+[+]−) and (−[+]+), are formally analogous yet in principle inequivalent, owing to the lack of centers of symmetry

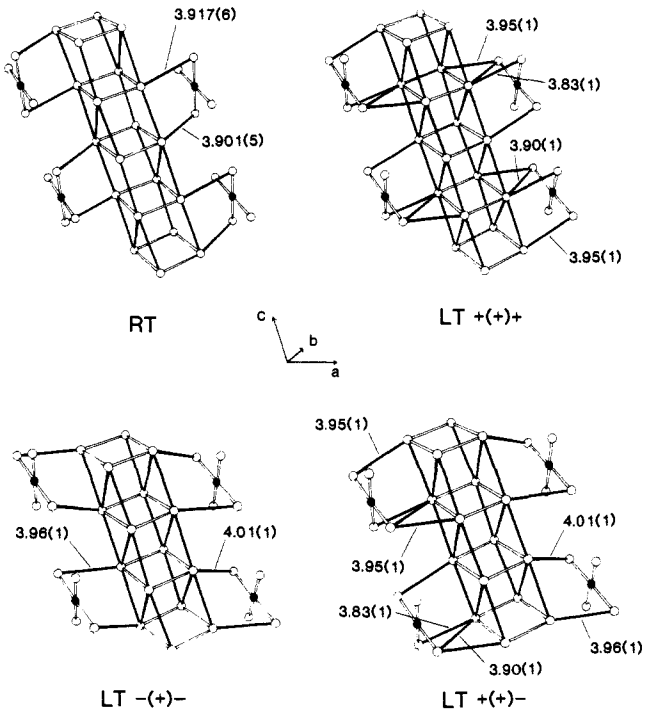

Figure 11. Comparison of the three different types of environments available to a TMTSF stack in the simplified low-temperature $[TMTSF]_2[Ni(tds)_2]$ structure with the single type of environment found in the corresponding room-temperature structure. In each case, the view is onto the *a–c* plane, as in Figure 8. For clarity, only the Ni (●) and Se (○) atoms are shown; intermolecular distances ≤4.0 Å are indicated as solid lines. Each Se···Se contact distance indicated is the average of two inequivalent distances in the actual low-temperature structure.

crystallographically imposed on ions in the low-temperature structure. But because the deviations of the observed ion geometries from perfect centrosymmetry are very small, we hereafter approximate each of the symmetry-independent ions within the low-temperature cell by an average, centrosymmetric equivalent. In the resulting simplified structure the interatomic distance for each anion–cation Se–Se contact is the average of the corresponding inequivalent distances in the observed low-temperature structure, and the (+[+]-) and (-[+]+) environments are equivalent.

The three unique types of environments in the simplified low-temperature structure are depicted for a TMTSF reference stack in Figure 11. The first of these, (+[+]+), is formally analogous to the single type of environment found for each stack and chain in the room-temperature structure. A hypothetical extended, ordered network of the type $([+]+]_x$ therefore exhibits a two-dimensional character similar to that found at room temperature. Close inspection of the stack–chain contacts within the *a–c* plane, however, reveals significant differences that result from the reorientation of the anions: there are *four* distinct types of short Se–Se contacts spanning each [+]+ interface, compared to only two such contacts in the analogous room-temperature interaction. One room-temperature type anion–cation contact (that with $d_{Se-Se}(RT) = 3.917$ (6) Å) not only is preserved but is significantly shortened (to 3.83 Å) in the low-temperature [+]+ interaction; the other is abolished (i.e., $d_{Se-Se}(LT) > 4.0$ Å). The loss of one room-temperature type contact, however, is more than compensated by the concomitant formation of three new types of short anion–cation Se–Se contacts.

The other two types of environments, namely (+[+]-) and (-[+]-), differ from the first by the incorporation of at least one [+]- interaction. This new type of stack–chain relationship dramatically alters the two-dimensional character of the low-temperature anion–cation network by interrupting the proliferation of the anion–cation interactions throughout the *a–c* plane. Thus, in a hypothetical $([+]-)_x$ network the short stack–chain Se–Se contacts would form one-dimensional $(anion–cation)_x$ chains along *a* that are not linked by any diagonal couplings.

Because the (+) and (-) elements are randomly distributed within the low-temperature structure, the effective two-dimensional character of the low-temperature phase is intermediate between those of the hypothetical $([+]+)_x$ and $([+]-)_x$ networks. For a given reference stack (or chain) and its two nearest neighbors, the probability of obtaining an arrangement containing at least one [+]- interface is 3 times that of obtaining the +[+]+ configuration. The $(anion–cation)_x$ network within the *a–c* plane of the low-temperature structure is therefore considerably more one-dimensional on average than that of the room-temperature structure. This qualitative alteration of the anion–cation interactions at the transition is accompanied by an increase in the average *number* of distinct types of short Se–Se contacts per stack–chain interface, from 2 (with average $d_{Se-Se} = 3.91$ Å) at room temperature to 3 (with average $d_{Se-Se} = 3.94$ Å) at low temperature. On the assumption that the Se–Se orbital overlaps associated with the room-temperature and low-temperature anion–cation interactions are comparable, this reflects a strengthening of the transverse coupling between adjacent stacks and chains within the *a–c* plane of the low-temperature phase. The possible significance of the reduced two-dimensional character in the low-temperature structure is discussed in the following section.

Discussion

We have previously reported[9] that the molecular conductors $[TMTSF]_2[M(tds)_2]$ (M = Ni, Pt) exhibit a novel, reversible phase transition in which the low-temperature phase shows enhanced conductivity. The crystal structure of these materials comprises conducting stacks of TMTSF molecules in close contact with chains of complex anions. Static magnetic susceptibility and ESR measurements confirm the formulation $[(TMTSF)^{0.5+}]_2[[M(tds)_2]^-]$. For M = Ni or Pt, each anion possesses an unpaired spin that is magnetically coupled to the charge carriers within the TMTSF-based conduction band. We have also described the preparation and physical characterization of the analogous Cu compound; of particular interest here is the observation that substituting Cu for Ni or Pt suppresses the transition. Since $[TMTSF]_2[Cu(tds)_2]$ is both isostructural (at room temperature) and isoionic with the corresponding Ni and Pt compounds, we infer that it is the different electronic character of the $[Cu(tds)_2]^-$ ion, compared to that of its Ni and Pt analogues, that is responsible for the strikingly different behavior.

Though historically a matter of some controversy, the electronic structures of complexes of this type are now well understood.[34] When M = Ni or Pt, the planar $[M(tds)_2]^-$ ion has an open-shell, paramagnetic ($S = {}^1/_2$) configuration. The unpaired electron resides in a molecular orbital of B_{3g} symmetry (in D_{2h}) that has substantial contributions from both the metal d_{xy} and ligand p_z orbitals. Analysis of the ESR spectra of the M = Ni and Pt monoanions in frozen solution[10] indicates that the orbital density on the Se atoms is ca. 0.1 per Se. In the corresponding monoanionic Cu complex, this orbital is doubly occupied, yielding a closed-shell, diamagnetic configuration. Because the HOMO of the $TMTSF^+$ cation also is centered largely upon the Se atoms,[35] short anion–cation Se–Se contacts in the solid state are expected to give rise to electronic interactions between the TMTSF stacks and the intervening anion chains within the *a–c* plane, and these interactions should be substantially stronger when the $[M(tds)_2]^-$ ions have an open-shell electronic structure (i.e., M = Ni or Pt) than when they have a closed-shell configuration (i.e., M = Cu).

Comparison of the room-temperature and low-temperature structures of $[TMTSF]_2[Ni(tds)_2]$ indicates that the 275 K structural transition alters and apparently strengthens the network of anion–cation Se–Se contacts in the low-temperature phase. Unfortunately, the lack of suitable crystals has prevented a parallel low-temperature structure determination on the corresponding Pt derivative; nonetheless, on the basis of the similarity of the

(34) Alvarez, S.; Vicente, R.; Hoffmann, R. *J. Am. Chem. Soc.* **1985**, *107*, 6253–6277, and references therein.
(35) Whangbo, M.-H.; Walsh, W. M.; Haddon, R. C.; Wudl, F. *Solid State Commun.* **1982**, *43*, 637–639.

physical properties of the two compounds, we infer that the structural modification associated with the 245 K transition in the Pt compound must be qualitatively similar to that of the Ni homologue. In both cases, we believe that a transition-induced enhancement of the anion–cation Se–Se interactions plays an important role in stabilizing the low-temperature structure. Conversely, the absence of a corresponding transition in the Cu homologue suggests that the weaker electronic interactions between the cations and closed-shell anion in this compound render such a structural modification energetically unfavorable. In short, we conclude that electronic factors supply the dominant driving force for the structural transition in these materials. It is not certain whether the observed low-temperature disordered structure actually represents the thermodynamically most stable state. It is conceivable that this structure in fact represents a metastable state quenched out by cooling through a kinetically sluggish transition.

Apart from the increase in $\sigma_{\parallel}$ accompanying the structural transition in M = Ni and Pt, the conductivities of all three compounds exhibit similar temperature responses, with metal-like character near room temperature but weakly activated at lower temperatures. Similar behavior has been found for a number of other molecular conductors,[19,35-39] and several 1-D band models have been proposed to account for it. These include (1) conduction via a thermally activated population of charge carriers that have strongly temperature-dependent mobilities[19] and (2) conduction via strongly correlated polarons.[37] The satisfactory fit of the M = Cu conductivity data to eq 1 is consistent with either of these mechanisms, but the appropriate interpretation of the resulting parameters is unclear given the apparent two-dimensional character of these materials. More importantly, the room-temperature structure of the isostructural Ni derivative provides no evidence of a static distortion that would open a gap at the Fermi level,[40] and neither model can successfully account for the observed Pauli-like behavior of the carrier spins.

An alternative model that appears to be consistent with the available physical and structural data involves dynamic Peierls' fluctuations of the conducting TMTSF stacks. This phenomenon has been well-documented in the family of partially oxidized tetracyanoplatinate salts,[35] which exhibit analogous conductivity behavior.

We now consider how the structural transition affects the conductivity of the Ni and Pt compounds. When the crystal is cooled through the transition, both $\sigma_{\parallel}$ and $\sigma_{\perp}$ increase by comparable amounts. Although the enhancement of $\sigma_{\perp}$ by the transition is consistent with the observed strengthening of the transverse anion–cation interactions in the low-temperature phase, there is no correspondingly simple explanation for the concomitant increases in $\sigma_{\parallel}$. Because the TMTSF stacks retain their room-temperature form below the transition, we infer that the alteration of the anion–cation couplings in the low-temperature structure is responsible for the improvement in $\sigma_{\parallel}$ as well. The increased interstack carrier mobilities resulting from the strengthened anion–cation couplings will enhance the ability of the charge carriers to bypass defects in the TMTSF stacks, thereby increasing $\sigma_{\parallel}$. To the extent that the conductivity remains one-dimensional, the disorder in the low-temperature phase might help to increase the conductivity by acting to suppress Peierls' fluctuations.

A possible influence of the crystal field inequivalence of different TMTSF stacks below the transition must also be considered. Such an effect is thought to be responsible for an analogous increase in conductivity that occurs below a 272 K structural transition in the organic semiconductor [DMTM][TCNQ]$_2$ (DMTM = *N*,*N*-dimethylthiomorpholinium).[41] The room-temperature structure of this compound consists of dimerized TCNQ stacks separated by sheets of cations; as in the [TMTSF]$_2$[M(tds)$_2$] compounds, the phase transition involves the vertical translation of parallel stacks relative to one another.

In [DMTM][TCNQ]$_2$ the presence of dimers causes a gap at the Fermi energy in the band structure of the TCNQ stacks, and it is a modification of this gap structure that gives rise to increased conductivity in the low-temperature phase. In contrast, the TMTSF stacks in the present compounds have a metallic band structure. In this case, the different environment of, for example, a (+[+]+) to a (-[+]+) stack does shift the band energy of one stack relative to the other; however, provided that the valence bandwidth is greater than the relative energy difference between bands on inequivalent stacks in the low-temperature structure, the metallic character will be preserved through the transition and the Fermi levels will be equalized by charge transfer between stacks. This implies that the degree of band filling for bands on the three different types of stacks within the low-temperature structure will be different, but the *average* band filling will be unchanged by the transition. The crystal field inequivalence of the TMTSF stacks therefore is not expected to perturb significantly the conductivity properties of the low-temperature phase.

The structural phase transition also affects the magnetic properties of the [TMTSF]$_2$[M(tds)$_2$] compounds. The Curie–Weiss susceptibilities of the localized anion species in the Ni and Pt compounds below the transition indicate that there are significant magnetic interactions among the anions in the low-temperature phase. Structural considerations suggest that an analogous, though qualitatively different, interaction is also present at room temperature. The lack of appreciable overlap between the [M(tds)$_2$]$^-$ ions within the sheets parallel to the *b*–*c* plane in both the room-temperature and low-temperature structures implies that the coupling occurs between anions belonging to different chains within the two-dimensional networks parallel to the *a*–*c* plane. Such coupling presumably arises via superexchange interactions mediated by the intervening TMTSF cations; the observation, by ESR spectroscopy, of exchange coupling between the anion and cation spin systems in [TMTSF]$_2$[Ni(tds)$_2$] is consistent with such a mechanism. Since the anion–cation contacts are significantly altered by the phase transition, we conclude that the subtle inflections or discontinuities in the magnetic behavior of these compounds at the transition reflect the influence of the structural reorganization upon the superexchange pathways.

At low temperatures, where the conductivity has become negligible ($\sigma < 10^{-3}$–10^{-4} Ω^{-1} cm^{-1}), the interactions among the anions give rise to magnetic transitions that remain to be fully characterized. Both the Ni and Pt compounds exhibit reduced susceptibilities, below 13 and 28 K, respectively, indicative of extended antiferromagnetic interactions among the localized anion species. The low-temperature structure suggests that the magnetic coupling has predominantly one-dimensional character; we therefore consider again the hypothetical ([+]–)$_x$ network (Figure 11) as a limiting case. In such a structure, superexchange interactions between only those pairs of anions that contact the same TMTSF cation leads to magnetic coupling within one-dimensional (anion–cation)$_x$ chains lying along *a*. At higher temperatures, where σ is appreciable, the presence of itinerant charge carriers associated with the TMTSF stacks could cause additional coupling along *c*, mediated by the carrier spins, between the one-dimensional chains of this type within the *a*–*c* plane. We have recently described[42] a similar coupling of localized moments via itinerant carrier spins in highly conducting Cu(pc)I.

Of course, the observed low-temperature structure does exhibit some branching of the anion–cation Se–Se contacts within the

(36) Williams, J. M. *Adv. Inorg. Chem. Radiochem.* **1983**, *26*, 235–268.
(37) Hoffman, B. M.; Phillips, T. E.; Soos, Z. G. *Solid State Commun.* **1980**, *33*, 51–54.
(38) Ashwell, G. J.; Chyla, A.; Heimer, N. E.; Metzger, R. M.; Allen, J. G. *Mol. Cryst. Liq. Cryst.* **1985**, *120*, 137–140.
(39) Coulon, C.; Delhaes, P.; Flandrois, S.; Lagnier, R.; Bonjour, E.; Fabre, J. M. *J. Phys.* (*Les Ulis, Fr.*) **1982**, *43*, 1059–1067.
(40) This system thus provides an interesting contrast to the analogous (tetrathiotetracene)$_{1.2}$[Ni(ethylene-1,2-dithioleno)$_2$] where it is believed that the periodic crystal field of the regular array of [Ni(edt)$_2$]$^-$ ions stabilizes such a distortion: Bray, J. W.; Hart, H. R.; Interrante, L. V.; Jacobs, I. S.; Kasper, J. S.; Piacente, P. A. *Phys. Rev. B: Solid State* **1977**, *B16*, 1359–1364.
(41) Visser, R. J. J.; Van Smaalen, S.; De Boer, J. L.; Vos, A. *Mol. Cryst. Liq. Cryst.* **1985**, *120*, 167–172.
(42) (a) Ogawa, M. Y.; Hoffman, B. M.; Lee, S.; Yudkowsky, M.; Halperin, W. P. *Phys. Rev. Lett.* **1986**, *57*, 1177–1180. (b) Ogawa, M. Y.; Martinsen, J.; Palmer, S. M.; Stanton, J. L.; Tanaka, J.; Greene, R. L.; Hoffman, B. M.; Ibers, J. A. *J. Am. Chem. Soc.* **1987**, *109*, 1115–1121.

a-c plane, owing to the occurrence of diagonal contacts associated with (+[+]+) environments; the relatively low probability and random distribution of these branching interactions within the two-dimensional networks, however, suggest that they are properly regarded as defects within predominantly one-dimensional magnetic chains along a. Physical studies on solid solutions of the type $[[TMTSF]_2Ni(tds)_2]_x[Cu(tds)_2]_{1-x}$ should provide further information about the magnetic properties of these compounds.

Acknowledgment. This work was supported by the Solid State Chemistry Program of the National Science Foundation (Grant DMR 85-19233 to B.M.H.) and by the Northwestern University Materials Research Center under the NSF-MRL program (DMR 85-20280). We further acknowledge Johnson Matthey Inc. for the loan of platinum salts.

Registry No. $[TMSF]_2[Ni(Tds)_2]$, 102784-07-6; $[TMSF]_2[Pt(tds)_2]$, 102764-53-4; $[TMSF]_2[Cu(tds)_2]$, 111557-31-4.

Supplementary Material Available: Tables of positional and anisotropic thermal parameters (2 pages); listing of structure amplitudes for both the room- and low-temperature structures (20 pages). Ordering information is given on any current masthead page.

Mechanism of Acyl Group Isomerization in Palladium(II) Complexes. Development of a Catalytic Process for the Isomerization of Carboxylic Acid Chlorides

Jeffrey S. Brumbaugh and Ayusman Sen*[1]

Contribution from Chandlee Laboratory, Department of Chemistry, The Pennsylvania State University, University Park, Pennsylvania 16802. *Received April 6, 1987*

Abstract: $[Pd(PPh_3)_2(MeCN)(CO^iPr)](BF_4)$ (**2c**), when dissolved in a variety of weakly coordinating polar solvents, spontaneously isomerized to an equilibrium mixture of **2c** and $[Pd(PPh_3)_2(MeCN)(CO^nPr)](BF_4)$ (**2d**). Several other complexes having the general formula $[Pd(PPh_3)_2(MeCN)(COR)](BF_4)$ also underwent spontaneous isomerization, including those involved in the following isomer systems: R = $^nBu/^tBu$, $^iBu/^tBu$, and methylcyclohexyl. In each system the more stable isomer was that having the least branching in the alkyl group. When R was a vinyl group, the complex decomposed to form the respective vinyltriphenylphosphonium salt. The reactions were first order in metal complex and inverse first order in MeCN. PPh_3 inhibited the reactions by promoting metal complex decomposition. When the isomerizations were carried out in the presence of an excess of ethylene or cyclohexene, $[Pd(PPh_3)_2(MeCN)(COEt)](BF_4)$ (**2b**) or $[Pd(PPh_3)_2(MeCN)(COC_6H_{11})](BF_4)$ (**2n**) respectively, was produced in high yields. Concomitant with the formation of **2b** in the reaction of $[Pd(PPh_3)_2(MeCN)(COC_7H_{13})](BF_4)$ with ethylene was the formation of methylenecyclohexane, 1-methylcyclohexene, 3-methylcyclohexene, and 4-methylcyclohexene. When the reaction was carried out in $CDCl_3$, a small quantity of $CHDCl_2$ was generated as a byproduct, arising from the reaction of an intermediate metal hydride with the solvent. A key intermediate in the reaction mechanism was postulated to be $[Pd(PPh_3)_2(H)(CO)(olefin)](BF_4)$, which was formed from the starting material via the following sequence of events: (a) MeCN dissociation, (b) CO deinsertion, and (c) β-hydrogen abstraction. The reversal of steps a-c generated the isomeric acyl compound. The corresponding neutral palladium-acyl complexes, $Pd(PPh_3)_2(Cl)(CO^iPr)$ and $Pd(PPh_3)_2(Cl)(CO^nPr)$, underwent isomerization to an equilibrium mixture of these isomers when a Lewis acid or $[Pd(PPh_3)_2(MeCN)(COR)](BF_4)$ was employed as a catalyst. Finally, the catalytic isomerization of isobutyryl chloride or *n*-butyryl chloride to an equilibrium mixture of these organic acids was promoted by either $[Pd(PPh_3)_2(MeCN)(COR)](BF_4)$ or a combination of $Pd(PPh_3)_2(Cl)(COR)$ and $AlCl_3$.

Transition-metal-acyl complexes are ubiquitous and those belonging to the later transition metals are actively involved in a large number of catalytic and stoichiometric carbonylation and decarbonylation reactions. These include the hydroformylation[2] and carbonylation[3] of olefins, the copolymerization of olefins with carbon monoxide,[4] the carbonylation of alcohols[5] and alkyl and aryl halides,[6] and the decarbonylation of aldehydes and carboxylic acid chlorides.[7] However, despite the central role played by metal-acyl complexes in these reactions, the question of their structural integrity has not been addressed in detail. The product regiospecificity in many of the above reactions will depend on the propensity toward acyl isomerization in the intermediate metal-acyl compounds (eq I).

$$M\text{-}COCHRCH_2R' \rightleftharpoons M\text{-}COCHR'CH_2R \qquad (I)$$

Prior to our work, the isomerization of the acyl group in $Co(CO)_4(COR)$[8] and $Rh(PPh_3)_2(CO)_2(COR)$[9] had been briefly reported; however, no mechanistic information was available concerning these systems. Herein, we report the results of our studies on the spontaneous acyl group isomerization in cationic palladium(II) complexes. These studies have also led to the development of a novel palladium-catalyzed process for the

(1) Alfred P. Sloan Research Fellow, 1984-1988.

(2) Reviews: (a) Cornils, B. In *New Syntheses with Carbon Monoxide*; Falbe, J., Ed.; Springer-Verlag: Berlin, 1980; p 1. (b) Pruett, R. L. *Adv. Organomet. Chem.* **1979**, *17*, 1. (c) Marko, L. In *Aspects of Homogeneous Catalysis*; Ugo, R., Ed.; Reidel: Dordrecht, 1974; Vol. 2, p 3.

(3) Review: Mullen, A. In ref 2a; p 243.

(4) (a) Sen, A. *Adv. Polym. Sci.* **1986**, *73/74*, 125. (b) Lai, T.-W.; Sen, A. *Organometallics* **1984**, *3*, 866. (c) Sen, A.; Lai, T.-W. *J. Am. Chem. Soc.* **1982**, *104*, 3520.

(5) (a) Dekleva, T. W.; Forster, D. *J. Am. Chem. Soc.* **1985**, *107*, 3565, 3568. Reviews: (b) Bahrmann, H.; Cornils, B. In ref 2a; p 226. (c) Drury, D. J. In ref 2c, 1984; Vol. 5, p 197.

(6) Reviews: (a) Heck, R. F. *Adv. Catal.* **1977**, *26*, 323. (b) Weil, T. A.; Cassar, L.; Foa, M. In *Organic Syntheses via Metal Carbonyls*; Wender, I., Pino, P., Eds.; Wiley: New York, 1972; Vol. 2, p 517. Leading references for the related "double carbonylation" of halides: (c) Ozawa, F.; Soyama, H.; Yanagihara, H.; Aoyama, I.; Takino, H.; Izawa, K.; Yamamoto, T.; Yamamoto, A. *J. Am. Chem. Soc.* **1985**, *107*, 3235. (d) Chen, J.-T.; Sen, A. *J. Am. Chem. Soc.* **1984**, *106*, 1506.

(7) Review: Tsuji, J.; Ohno, K. *Synthesis* **1969**, 157.

(8) (a) Ungvary, F.; Marko, L. *Organometallics* **1982**, *1*, 1120. (b) Masada, H.; Mizuno, M.; Suga, S.; Watanabe, Y.; Takegami, Y. *Bull. Chem. Soc. Jpn.* **1970**, *43*, 3824. (c) Takegami, Y.; Watanabe, Y.; Masada, H.; Okuda, Y.; Kubo, K.; Kokokawa, C. *Bull. Chem. Soc. Jpn.* **1966**, *39*, 1495. (d) Takegami, Y.; Yokokawa, C.; Watanabe, Y. *Bull. Chem. Soc. Jpn.* **1966**, *39*, 2430. (e) Takegami, Y.; Yokokawa, C.; Watanabe, Y.; Masada, H.; Okuda, Y. *Bull. Chem. Soc. Jpn.* **1965**, *38*, 787. (f) Takegami, Y.; Yokokawa, C.; Watanabe, Y.; Okuda, Y. *Bull. Chem. Soc. Jpn.* **1964**, *37*, 181. (g) Takegami, Y.; Yokokawa, C.; Watanabe, Y.; Masada, H.; Okuda, Y. *Bull. Chem. Soc. Jpn.* **1964**, *37*, 1190. (h) Rupilius, W.; Orchin, M. *J. Org. Chem.* **1972**, *37*, 936.

(9) Brown, J. M.; Kent, A. G. *J. Chem. Soc., Chem. Commun.* **1982**, 723.

0002-7863/88/1510-0803$01.50/0